Very High-Temperature Impact Melt Products as Evidence for Cosmic Airbursts and Impacts 12,900 years ago

SUPPORTING INFORMATION: IMAGES

HYPERLINKS:

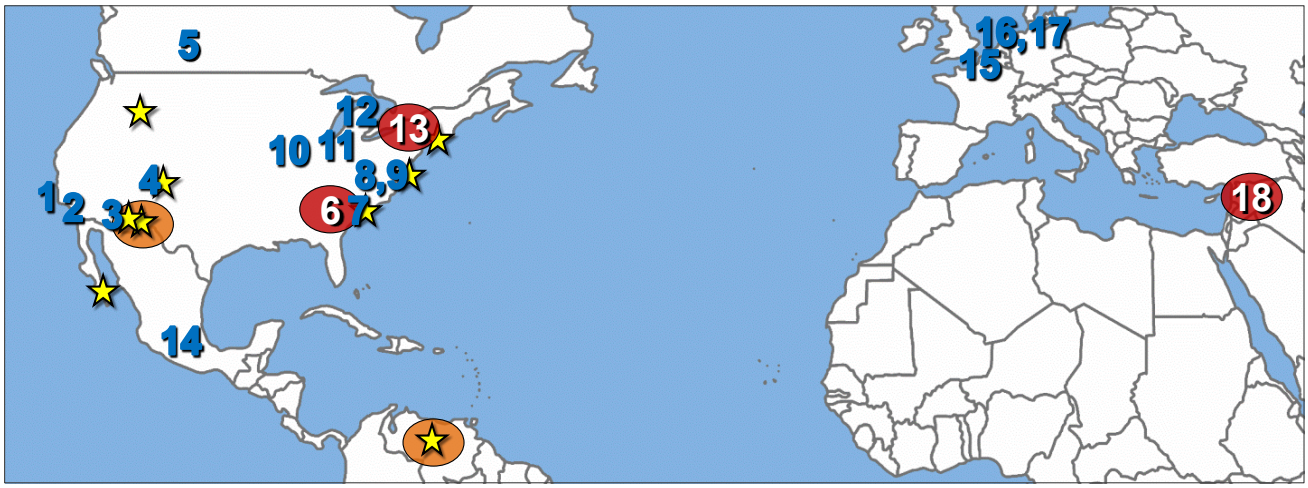

Figure S1. Site Map for 18 numbered sites in this study (described below), spanning about 12,000 km of the Northern Hemisphere. Currently, there is no known limit to the YDB impact field.

SLOs and spherules were observed at the three numbered sites in red circles: (#6) Blackville, South Carolina; (#13) Melrose, Pennsylvania; and (#18) Abu Hureyra, Syria.

Impact-related spherules without SLOs were observed at the other sites numbered in blue as follows: (#1) Arlington Canyon, California; (#2) Talega, California; (#3) Murray Springs, Arizona; (#4) Blackwater Draw, New Mexico; (#5) Chobot, AB, Canada; (#7) Topper, South Carolina; (#8) Barber Creek, North Carolina; (#9) Kimbel Bay, North Carolina; (#10) Big Eddy, Missouri; (#11) Sheriden Cave, Ohio; (#12) Gainey, Michigan; (#14) Cuitzeo, Mexico; (#15) Lommel, Belgium; (#16) Ommen, Netherlands; and (#17) Lingen, Germany.

Independent research. Also shown are 9 sites (yellow stars) investigated by 7 independent groups. SLOs were found at two sites, marked with a star in orange circle: Venezuela (Mahaney *et al.*, 2011) and Arizona (Fayek *et al.*, 2008, 2011). Impact-related YDB microspherules without SLOs were reported in the YDB layer in Montana (Baker *et al.*, 2008); Arizona (Haynes *et al.*, 2010); Mexico (Scruggs *et al.*, 2010); New Mexico, Maryland, South Carolina (LeCompte *et al.*, 2010); and Pennsylvania (Wu *et al.*, 2011).

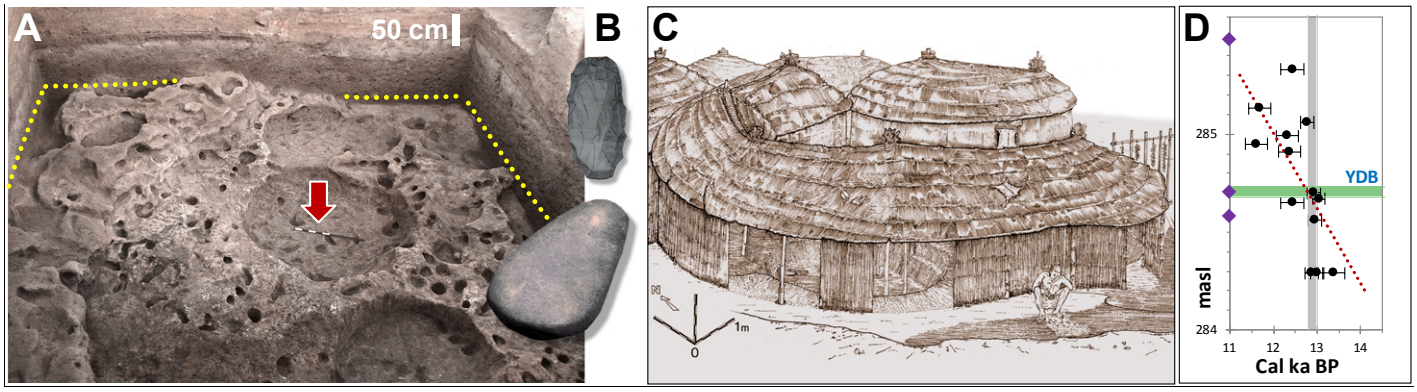

Figure S2. Abu Hureyra, Syria. A) This site is located on an archaeological mound, or "tell," about 14 km west of Al Thawra, Syria (lat/long: 35.8667°N, 38.4000°E)**.** The site was excavated shortly before being flooded by the filling of Lake Assad in 1974. Sediment samples and archeological collections are curated at the University College London, but the site remains submerged >25 m below the lake surface. Trench E, 7×7 m square (shown above) displayed circular floor depressions that are all that remains of pit-houses used by inhabitants at 12.9 ka. The YDB layer is represented by the yellow dotted line. **B)** A 60-cm grinding stone (bottom), found inside the pit-house at red arrow, dates to the YDB, and was used to process food grains, when the villagers began cultivating plants including a domesticated variety of rye (Moore *et al.*, 1986, 2000; Moore and Hillman, 1992; Hillman *et al.*, 2001). At center top is an illustration of an 8-cm flaked stone tool from approximately the same level as the grindstone. **C)** Illustration of thatched pit-houses used at 12.9 ka by hunter-gatherers in a village covering approximately 2000 m^2. **D)** Linear interpolation is used to develop an age-depth model based on 13 accelerator mass spectrometry (AMS) radiocarbon dates from Moore *et al.* (2000) (red dotted line) (**SI Table 2**). The vertical gray bar represents 12.9 ± 0.1 ka, and the purple diamonds represent sediment sampling locations. The green bar shows the depth of the peaks in SLOs and spherules in Level 445 (see Figure S3), a 3-cm-thick layer centered at 284.7 above sea level (asl) from 284.69 and 284.72 m asl at 4.1 m below surface (mbs) (**Figure S3)**. Based on linear interpolation, the YDB layer is within the 12.9-ka age range.

Abu Hureyra Site; Stratigraphy and the YDB. Much of northern Syria consists of calcareous Mediterranean, steppe, and desert soils, all of which are enriched in CaO and SiO_2. This site is near the Euphrates River on well-developed, unconsolidated limey, silty sand, atop massive limestone deposits. Six samples of bulk sediment were examined over a 3.02-m interval from 287.6 to 284.58 m asl, as shown in **Figure S3**, exhibiting an average composition of SiO_2 at 31 weight percentage (wt%), CaO at 26 wt%, FeO^T at 12 wt%, and Al_2O_3, at 11 wt% (**SI Table 4**). The six samples display negligible compositional differences, except for the presence of higher carbon content from charcoal and ash in Level 445, excavated from just outside a pit-house (**Figure S3)**. All such YD-aged pit-houses at Abu Hureyra and their immediate environs contained a dark charcoal-rich layer indicating extensive burning that the excavators previously attributed to residue from cooking fires (Moore *et al.*, 2000), but which is also consistent with broader-scale biomass burning at 12.9 ka. Level 445 was a 3-cm-thick layer (yellow dotted line in **Figure S2A**), centered at 4.1 mbs or 284.7 m asl, relative to a local reference elevation. In addition to an abundance peak in charcoal, Level 445 contained major peaks in spherules (595/kg) and SLOs (15.8 g/kg; the highest of any site investigated), consistent with being the YDB layer.

The palynological and macrobotanical record at the site demonstrates that Level 445 coincides with major climatic change, previously interpreted to represent the onset of the Younger Dryas cooling episode (Moore *et al.*, 2000; Hillman *et al.*, 2001). At that time the regional environment of Abu Hureyra abruptly changed from a moist woodland-steppe to an arid, treeless steppe. This change is reflected by the sudden decline in abundance of charred seed remains of several major groups of food: (a) a decline of approximately 100% in seeds of food plants, such as wild pears and cherries, found in an oak-dominated park-woodland, which disappeared from the Abu Hureyra area at the YD onset; (b) a decline of approximately 70% in seeds of some legumes; and (c) a decline of approximately 60% in grains of wild ryes and wheat (Hillman *et al.* 2001). Altogether, changes in more than 150 species of plants reflect the major effects of this abrupt climatic change from warmer, moister conditions of the Bølling-Allerød episode to cooler, dryer condition at the onset of the YD at 12.9 ka. This climatic change coincides with deposition of SLOs and impact-related spherules in the YDB layer at Abu Hureyra.

Lateral Distribution of SLOs. To examine the lateral extent of the SLOs at Abu Hureyra, we sampled about 4.5 m away in the stratum above the YDB layer (levels 402-406) and observed about 0.23 g/kg of SLOs. This indicates that the SLOS are not limited to just one small area of the excavation trench.

Chronology and the YDB layer. We have adopted the chronology for Trench E of Moore *et al.* (2000), who acquired AMS radiocarbon dates on charcoal and charred bones, seeds, and grains (SI Table 2). Those authors collected non-contiguous samples in Trench E from various locations across 1.66 m of sediment ranging from about 284.24 to 285.90 m asl. For those samples, 13 AMS ^{14}C dates were acquired, ranging from 11.45 ± 0.30 ^{14}C kiloannum before present, or ka BP (13.37 ± 0.30 calibrated

kiloannum before present, or cal ka BP) to 10.60 ± 0.20 ^{14}C ka BP (12.43 ± 0.27 cal ka BP) (**SI Table 2**; Moore *et al.*, 2000). Based on linear interpolation of 13 ^{14}C dates, the 3-cm-thick proxy-rich YDB layer at Level 445 at 284.7 m asl (**Figure S3**) dates to 12.9 ± 0.15 ka, consistent with the age of the YDB at other sites.

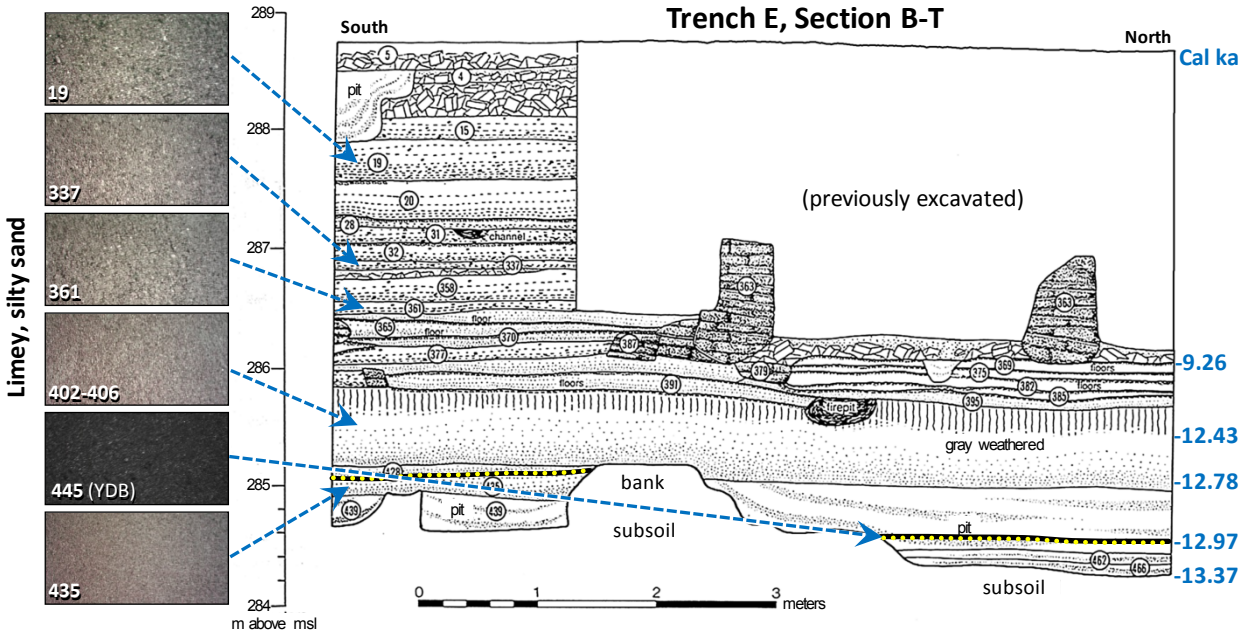

Figure S3. Cross-section diagram, matching the far wall of Trench E, shown in **Figure S2A.** "Bank" in this diagram corresponds to the highest point of the floor in the far wall in **Figure S1A.** Photomicrographs at left show colors of bulk sediment from the samples analyzed. Arrows point to the position of each sample in stratigraphic profile. The uniquely dark, charcoal-rich Level 445 (yellow dotted line, equivalent to yellow line in **Figure S2A**) displays peaks in SLOs and spherules. The YDB layer marking the onset of YD cooling at 12.9 ka is shown relative to the scale at right displaying five radiocarbon dates in cal ka BP, listed in **SI Table 2**.

Archaeological Importance of Abu Hureyra Site. This site in the Euphrates Valley in northern Syria is significant because it documents how and when hunter-gatherers in Western Asia began to cultivate domesticated plants, a fundamental step towards transforming human societies in the region during subsequent millennia (Moore *et al.*, 2000). Abu Hureyra is at present the oldest known site in the world demonstrating the transition from hunting-gathering to cultivation. Most final Epipalaeolithic hunter-gatherer and early Neolithic agricultural sites in Western Asia were located in separate places because of the different ecological requirements of these contrasting ways of life, and this has made it difficult to trace the course of the transition. Abu Hureyra, however, was inhabited relatively continuously from the Late Glacial into the early Holocene because it offered resources appropriate for both groups. The site's unusually lengthy occupation (6 kyrs from 13.4 to 7.5 ka) spanned major changes in climate and vegetation that are clearly visible in the archaeological record from the site and are connected to world-wide abrupt environmental adjustments during the Pleistocene-Holocene transition.

At the onset of the Bølling-Allerød episode at 14.6 ka, during what is called Phase 1 at Abu Hureyra, the climate across Western Asia, as elsewhere, began to ameliorate as temperatures rose and rainfall increased (Renssen *et al.* 2001; Robinson *et al.* 2006). This change stimulated an expansion of open woodland and grassland from the Mediterranean coast eastwards into the interior, creating highly favorable conditions for Late Glacial hunter-gatherers, whose numbers increased as a consequence (Moore *et al.,* 2000). The foragers who established the settlement at Abu Hureyra were attracted by an unusual array of resources, because the site lay at the edge of the Euphrates floodplain, giving easy access to two environmental zones, the river valley bottom and the woodland-steppe beyond, both important for the wild plant foods they offered. Furthermore, the site lay on a gazelle migration route that offered a rich seasonal meat source for the inhabitants. This abundance of edible wild plants and animals enabled the inhabitants to live at the site year-round, and therefore, they became sedentary hunter-gatherers for a few centuries.

During Phase 2 at Abu Hureyra, the beginning of which coincides with drier and cooler climate at the onset of the Younger Dryas at 12.9 ka, the vegetation around the site altered markedly as open woodland was replaced by arid steppe. This sudden change is documented in the plant remains recovered from the site itself and, more generally, in regional pollen core sequences (Moore and Hillman, 1992). Across large areas of Western Asia, patterns of settlement and economy among contemporary hunter-gatherer groups were disrupted. At Abu Hureyra, however, the inhabitants adopted farming at 12.9 ka while continuing to exploit wild plant and animal foods. Their crops included rye, lentils, and einkorn wheat (literally "single grain"), enabling them to maintain year-round occupation of the village.

In the following millennia, the villagers developed a

mature farming system from this nascent agricultural economy. They added more crops to the mix, including barley, bread wheat, and chickpeas, and also the main species of domestic animals, first, sheep and goats and then later, cattle and pigs. Sedentary village life supported by productive farming enabled the population to increase, such that in its later stages, Abu Hureyra had several thousand inhabitants and covered up to 16 hectare. The effects of this new way of life are clearly recorded archaeologically, including evidence for increased population size, the reorganization of the village layout, and new forms of houses. Also, the hard work required for growing and processing food was reflected in the skeletons of the people buried on site.

The adoption of plant cultivation at Abu Hureyra was caused by the convergence of several factors, one of which was the increase in the number of hunter-gatherers across the region, occasioned by an ameliorating environment towards the end of the Pleistocene. However, the catalyst for the ultimate adoption of plant cultivation was the rapid onset of the Younger Dryas and the disruption it caused. Only by adopting plant cultivation could the already-sedentary inhabitants of Abu Hureyra remain in place and maintain their settlement. We can now identify the Younger Dryas cooling event, felt widely across the planet, as a causal mechanism for the changes at Abu Hureyra, including the beginnings of domesticated plant cultivation.

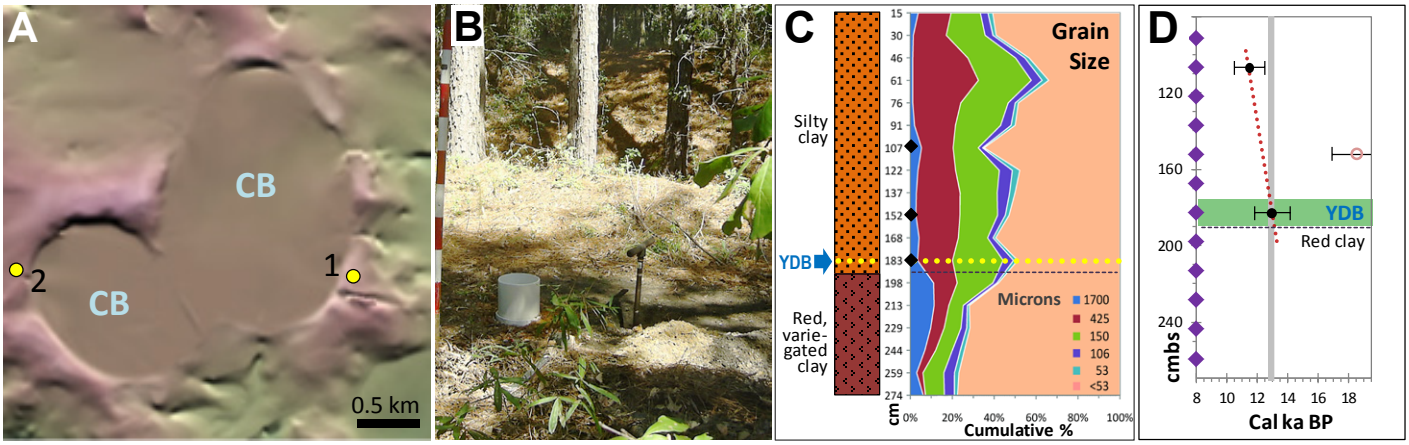

Figure S4. Blackville, SC. Core #1. A) The sampling site is about 3.2 km WNW of the town of Blackville (lat/long: 33.361545°N, 81.304348°W). The digital elevation model shows area topography, including several Carolina Bays (CB). Eighteen samples were acquired by coring from the widest and thickest part of the rim of a bay (core #1). **B)** Photo of sampling location with handle of core auger visible. **C)** Lithostratigraphy of section and sediment grain size distribution. Optically stimulated luminescence (OSL) sample depths in cm below surface (cmbs) are denoted by black diamonds; top of clay section is denoted by black dashed line. **D)** OSL dates place the onset of the YD at 12.9 ka in the sample centered at 183 cmbs (174 to 190 cm). Linear interpolation is used to develop an age-depth model (red dotted line) based on two OSL dates (**SI Table 2**). The vertical gray bar represents 12.9 ± 0.1 ka, and sediment sample locations are represented by purple diamonds. The green bar shows the depth of the peaks in SLOs and spherules in the 15-cm sample centered at 183 cmbs. Based on linear interpolation, the YDB layer is within the 12.9-ka age range.

Blackville Site. Stratigraphy and the YDB layer in Core #1. According to USGS maps (Horton and Dicken, 2001), the geologic profile for Blackville includes unconsolidated Quaternary alluvium over ~1-million-year-old Miocene marine clay. At the site, the surficial sediments are eolian and alluvial sediments comprised of variable loamy to silty red clays down to 190 cmbs. Immediately beneath 190 cmbs, there is massive, variegated, red clay, interpreted to be a paleosol that predates bay rim formation. There is an unconformity at this level, supported by the sharp increase from approximately 50% to 80% in fine-grained sediments (<53 μm), which increase with depth beginning at 190 cmbs and continuing to 274 cmbs (**Figure S4C**). Eighteen contiguous 15-cm-thick core samples of bulk sediment were examined from the surface to 274 cmbs, showing an average composition in the YDB layer of SiO_2 at 61 wt%, FeO^T at 10 wt%, and Al_2O_3 at 21 wt% (**SI Table 4**). Eleven samples were examined for SLOs and spherules, revealing a peak in SLOs (0.06 g/kg) and spherules (525/kg) in the 15-cm-thick interval centered at 183 cmbs (**SI Tables 2 & 3**).

Lateral Distributions of SLOs. At Blackville, we sampled the same stratigraphic level about 10 m away from the first location and observed about 0.02 g/kg of SLOs, comparable to abundances in core #1 (0.06 g/kg). This indicates that the SLOS are not limited to just one small area of the site. To further investigate the local distribution of YDB objects, Scott Harris extracted core #2 from an adjacent Carolina Bay rim 2.2 km to the west (lat/long: 33.364134°N, 81.328086°) and recovered 19 samples down to 163 cmbs. As in core #1, the sediments were mostly variable loamy to silty red clays, unconformably overlying massive red clay at 110 cmbs. We observed a broad peak in spherules (180/kg) from 80 to 100 cmbs, significantly lower in abundances than in core #1 (525/kg). No SLOs were observed. These results show a) that abundances of spherules are widespread in the area, but vary significantly over short distances, and b) that SLOs have highly variable local distribution and are absent in some places.

Chronology and the YDB layer. Because of a dearth of datable charcoal and because of sediment mixing

by deep-rooted plants, a recognized problem in this region (Casson and Feathers, 2001), radiocarbon dating of the YDB layer was not possible. Consequently, OSL dating of three samples was undertaken with the limited objective of testing whether the age of the layer containing SLOs and spherules is consistent with an age of 12.9 ka. Limitations of the OSL method include wide uncertainties of >1000 years, typically larger than for ^{14}C dating. The dating methodology required multiple small aliquots comprised of approximately100 quartz grains for each sample (Murray and Wintle, 2000). Standard practice was used at the OSL laboratory (IIRMES, California State University Long Beach) to obtain an average age for the sediment samples (Feathers, 2003).

OSL dating was conducted on three samples, including one centered at 183 cmbs in the layer containing peaks in SLOs and spherules. The dates obtained were 12.96 ± 1.19 ka at 183 cmbs, 18.54 ± 1.68 ka at 152 cmbs, and 11.5 ± 1.03 ka at 107 cmbs at 1σ probability (**SI Table 1**). The OSL age of 12.96 ka for the 183-cm, proxy-rich layer corresponds to the YDB age of 12.9 ka ± 010 ka, as published by Firestone *et al.* The two dates at 107 and 183 cmbs were used to generate an age-depth model, excluding the sample at 152 cmbs because of the large magnitude of the age reversal, i.e., older sediments lying stratigraphically higher than younger sediments. The age of the proxy-rich layer is consistent with the YDB age at other sites.

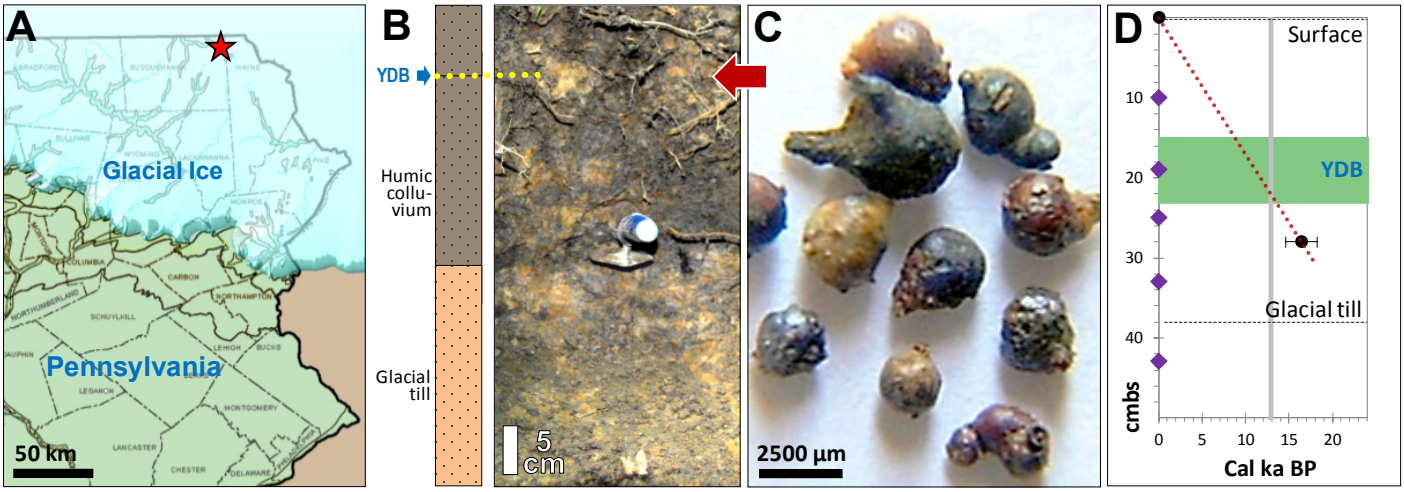

Figure S5. Melrose, PA. **A)** Area map showing location of the site (red star) about 1 km SW of the town of Melrose in northeastern PA (lat/long: 41.925350°N, 75.510066°W). The map shows the extent of glacial advance of the Laurentide Ice Sheet at approximately 25 ka (Fullerton *et al.* 2003) and began to retreat rapidly after 18 ka (Colgan *et al.*, 2003). **B)** Photo of exploratory trench showing lighter-colored glacial till (diamicton; below trowel), overlain by darker humic colluvium (photo credit: Malcolm LeCompte). The YDB is located in the colluvium in an 8-cm-thick layer from 15 to 23 cmbs, centered at 19 cmbs. **C)** Photomicrographs of subrounded SLOs ranging from about 800 to 5000 µm recovered from the YDB layer. These objects display evidence of melting at >2000°C, including lechatelierite (main paper, **Fig. 5C**), schlieren (**Fig. 16B**), impact pitting (**Fig. 6A**), and melt drapings (**Fig. 16D**) that conclusively rule out an origin by anthropogenesis, volcanism, or authigenesis. **D)** Linear interpolation is used to develop an age-depth model (red dotted line) based on one OSL date at 28 cmbs and the inferred age of surface sediments (**SI Table 2**). The vertical gray bar represents 12.9 ± 0.1 ka, and sediment sample locations are represented by purple diamonds. The green bar shows the depth of the peaks in SLOs and spherules in the 8-cm sample centered at 19 cmbs. Based on linear interpolation, the YDB layer is within the 12.9-ka age range.

Melrose site. Stratigraphy and the YDB layer. During the Last Glacial Maximum, the Melrose area in NE Pennsylvania lay beneath 0.5 to 1 km of glacial ice that reached maximum extent at approximately 25 ka and began to retreat rapidly after ~18 ka (Colgan *et al.*, 2003). According to the USGS (Berg *et al.*, 1980), the general geologic profile for Melrose is unconsolidated Quaternary alluvium over Pleistocene glacial till over the Devonian Catskill formation, comprised of sandstone, siltstone, shale, and mudstone. At this site, a shallow reconnaissance trench was excavated, and five contiguous samples were taken from 5 cmbs down to a depth of 48 cmbs. The sedimentary profile consists of fine-grained, humic colluvium down to 38 cmbs, resting on well-defined end-Pleistocene glacial till (diamicton, Figure S5B), comprised of 40 wt% angular clasts >2 mm in diameter. Bulk sediment showed an average composition of SiO_2 at 56 wt%, FeO^T at 11 wt%, and Al_2O_3 at 19 wt% (**SI Table 4**). Major abundance peaks in SLOs (0.8 g/kg) and spherules (3100/kg) occurred in an 8-cm-thick interval at 19 cmbs from 15 to 23 cmbs about 15 cm above the till, consistent with emplacement after 18 ka when the ice sheet retreated.

Lateral Distribution of SLOs. At Melrose, we sampled the same stratigraphic level above glacial till about 28 m away from the original sampling location. We found SLOs in about the same abundance (approximately 0.5 g/kg) as at the main site. To investigate whether SLOs are distributed more widely, we examined a forested site 28 km SSE from Melrose (41.698N, 75.347W). The site was selected because it was known to have been glaciated

(Fullerton *et al.* 2003), the topography was similar to that at Melrose, and the site is currently undisturbed by agricultural activities. Inspection revealed the sediment to be humic colluvium, containing angular clasts consistent with reworked glacial material. We extracted one 15-cm-thick sample across the interval from 15 to 30 cmbs, spanning the same 8-cm-thick interval as the YDB layer at Melrose (15 to 23 cm). Processing revealed that the sample contained >0.5 g/kg of SLOs up to 2 mm in diameter compared to 0.8 g/kg at Melrose, along with 2500 spherules/kg compared to 3100/kg. These results indicate that for these two sites a) abundances of SLOs and spherules are similar even though separated by 28 m and up to 28 km, and b) SLOs in the area are not limited to the Melrose site, although there are insufficient data to determine the extent of coverage.

Chronology and the YDB layer. Because of a dearth of datable charcoal at Melrose and because of sediment mixing by deep-rooted plants, as at Blackville, it was not possible to acquire direct radiometric dating of the sedimentary profile. Instead, we collected a sample for OSL dating at 28 cmbs, 5 cm below the layer containing peaks in SLOs and spherules (see approaches described earlier for the Blackville site). The sample yielded an OSL date of 16.4 ± 1.6 ka (**SI Table 2**), and assuming a modern age for the surface layer, then linear interpolation dates the proxy-rich YDB layer centered at a depth of 19 cmbs to 12.9 ± 1.6 ka. This date is supported by its location relative to the glacial till known to date to <18 ka (Colgan *et al.,* 2003) and is consistent with a YDB age.

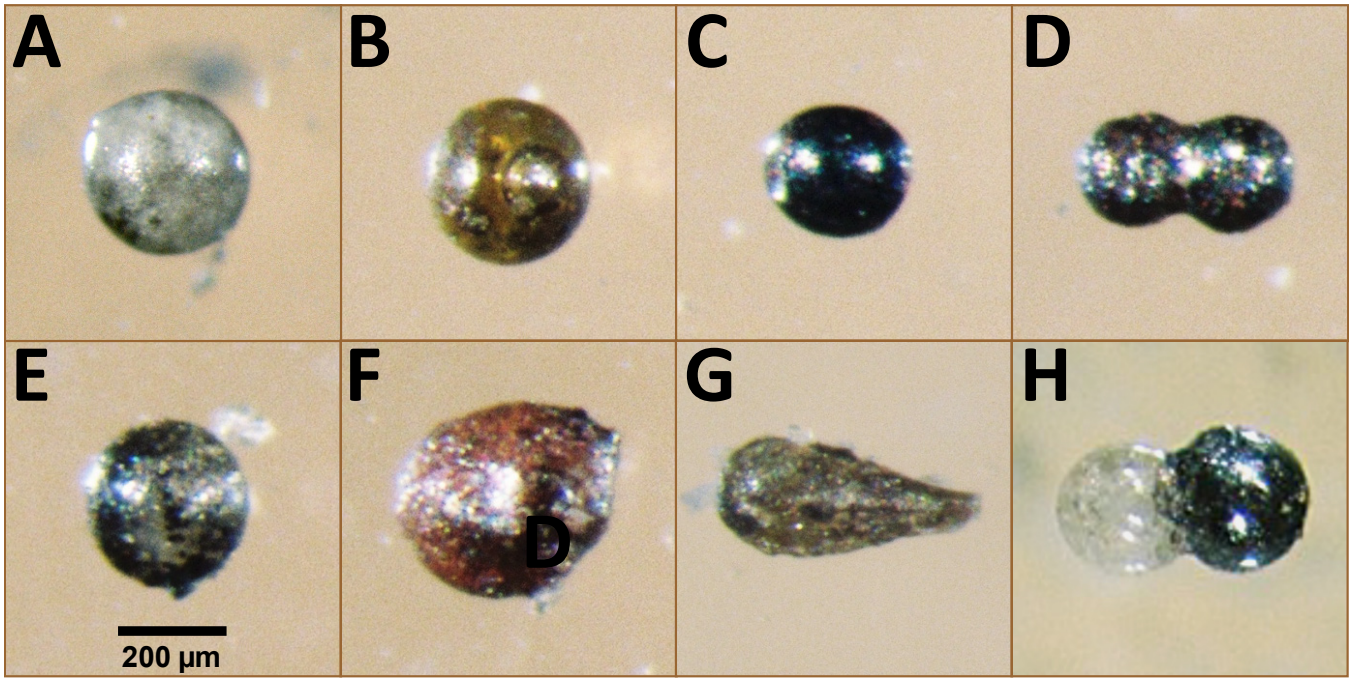

Figure S6. Light photomicrographs of magnetic and glassy spherules from Melrose, PA. Shapes include spherules, ovals, teardrops, and dumbbells. Colors include clear, gray, red, brown, and black. Note spherule **B** contains a large bubble. Both dumbbells (**D** and **H**) indicate fusion of molten or semi-plastic spherules. Note that dumbbell **H** consists of two dissimilar accretionary spherules, one clear (Si-rich) and the other opaque (Fe-rich).

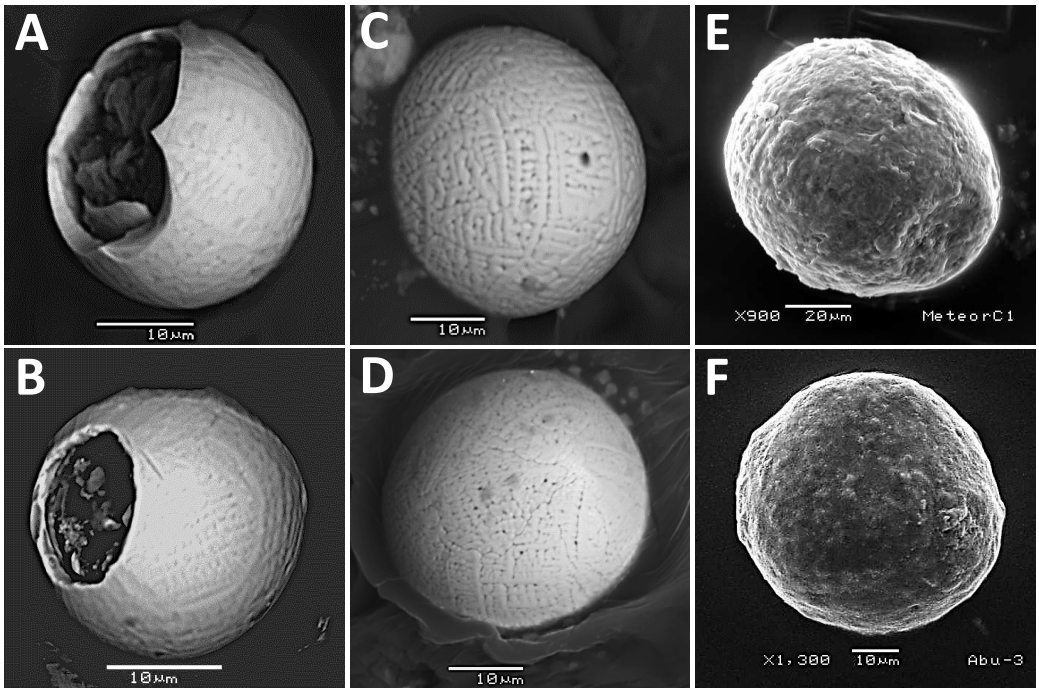

Figure S7. SEM images comparing YDB spherules with those of known impact events. **A)-B) KPg vs. YDB.** These images compare a spherule from the 65-Ma KPg boundary at Knudsens Farm, Canada with one from the YDB at Lake Cuitzeo, Mexico. These images are similar to those previously published of KPg spherules (Grachev *et al.*, 2008) and geochemically match other YDB spherules. **C)-D) Tunguska vs. YDB.** These images compare a spherule from the Tunguska, Siberia airburst of 1908 with one from the YDB at Lingen, Germany. Even though the Tunguska impactor did not produce a crater (Kulik, 1940), researchers have reported chemical traces of the impactor (Kolesnikov, 2010) and an abundance of spherules that formed during this event (Florenskiy, 1965). **E)-F) Meteor Crater vs. YDB.** These images compare a Fe-Ca-Si spherule from Meteor Crater, Arizona that formed in carbonate-rich rock with a Fe-Ca-Si spherule from Abu Hureyra, Syria that was also formed from carbonate-rich rock.

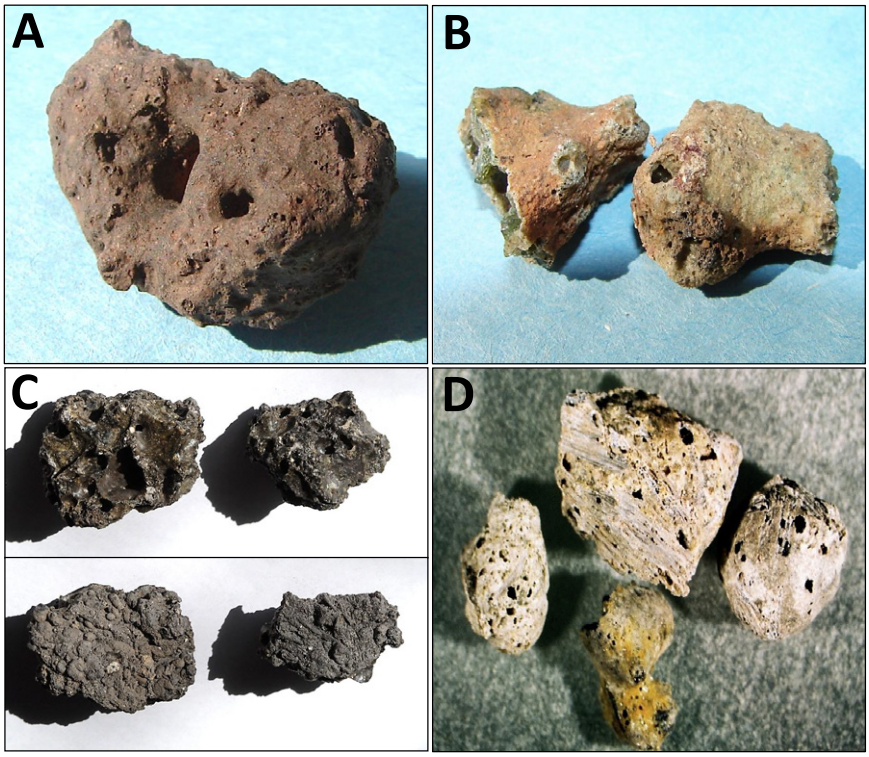

Figure S8. Light photomicrographs of high-temperature melt-glass. **A) Meteor Crater** SLO, width = 27 mm. **B) Trinity nuclear test, New Mexico, 1945**; yield 20 kilotons (kt). Glass known as trinitite; width =28 mm. **C) Soviet-era nuclear test, 1953;** material from Semipalatinsk, Kazakhstan. SLOs called "Stalinite" are from nuclear airburst with yield of 400 kt, TNT equivalent. Upper row formed facing up; lower row is down side of same objects. Width = 5.5 cm for largest. **D) Abu Hureyra** SLOs, width = 1 cm.

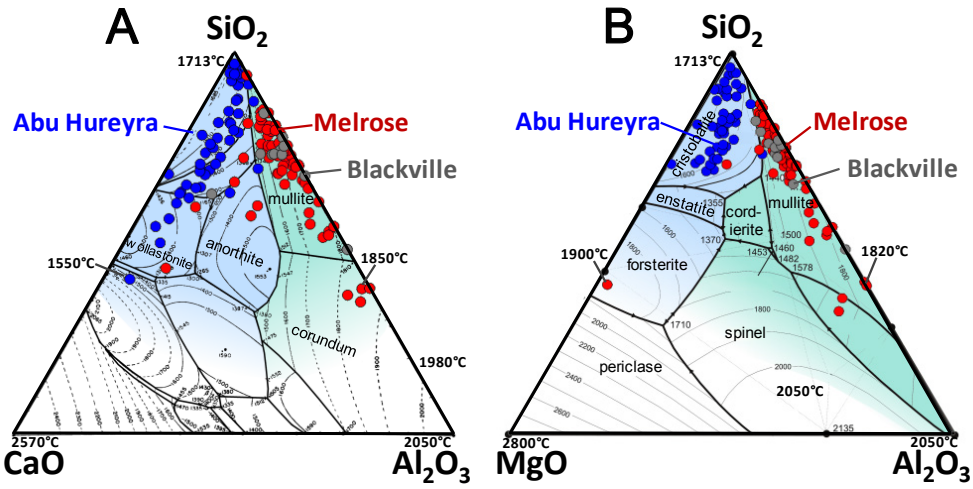

Figure S9. Temperatures. Ternary diagrams for estimated maximum temperatures of YDB objects. Key temperatures are displayed at each diagram corner and adjacent to the highest temperature sample for each group. The temperatures displayed are estimates only, because YDB objects contain significant amounts of iron (range: 0 to 100 wt%; mean: 55 wt%), which melts at lower temperatures. Overall, based on the temperature data here and in **Fig. 3D**, YDB objects belong to three main mineral groupings: 1) iron-rich, 2) aluminosilicate, and 3) Mg-and-Ca-aluminosilicate.

Ca-Silicate Sub-groups /Temperatures (Figure S9A). Using the standard CaO-Al_2O_3-SiO_2 (CAS) system, this ternary diagram indicates that YDB objects fall into two main groups, calcium-silicates and aluminosilicates. YDB objects from Abu Hureyra (blue dots) fall mostly in the CaO-SiO_2 group with liquidus temperatures up to 1700°C. Samples from Melrose (red dots) and Blackville, SC (gray dots) are mostly in the Al_2O_3-SiO_2 group that forms at temperatures up to 1850°C. Only a few YDB examples from Melrose and Blackville fall within the CaO-SiO_2 group.

Mg-Silicate Sub-groups/Temperatures (Figure S9B). The MgO-Al_2O_3-SiO_2 system shows that few Mg-rich silicate rocks are represented in YDB objects. Abu Hureyra (blue dots) falls mostly in the MgO-SiO_2 group, although Melrose (red dots) has several YDB objects that fall within the forsterite mineral region with melt temperatures of 1900°C. For the Al_2O_3-SiO_2 group, several Melrose YDB objects have maximum temperatures of 1820°C to 2050°C and fall within the mullite and corundum regions respectively, whose crystals have been observed using SEM.

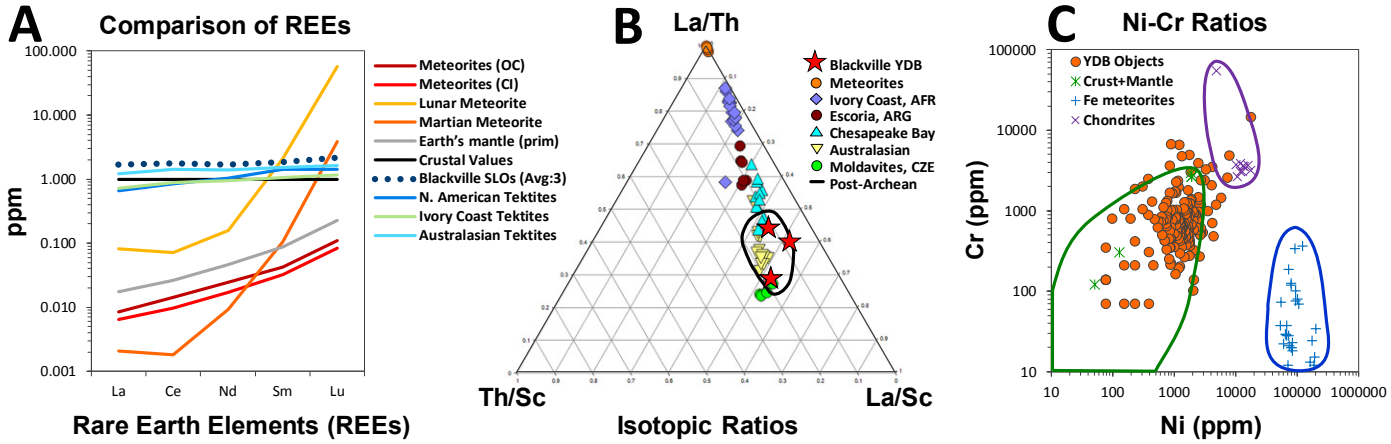

Figure S10. YDB objects derived from terrestrial precursors.

Crust-normalized rare-earth elements (REE) (Figure S10A). This graph compares values of REEs from Blackville SLOs to various other materials. REE compositions indicate SLOs from Blackville are compositionally comparable to tektites and to Earth's upper continental crust. SLOs are highly dissimilar to approximately 90% of all meteorites (OC, CI, Lunar, and Martian), and to material originating in Earth's mantle. This confirms that the YDB objects are terrestrial in origin, rather than cosmic. [Data sources: YDB from Firestone *et al.,* 2007, 2010. Meteorites from Lodders and Fegley, 1998; Gnos *et al.,* 2004; and Taylor *et al.*, 2002. Tektite data from Koeberl and Glass, 1988; Luetke *et al.*, 2008; and Lee *et al.*, 2004. Crust and mantle data from Taylor and McClennan, 1985]

Ratios of thorium, lanthanum, and scandium (Figure S10B). This ternary diagram further confirms that ratios for Blackville YDB objects are dissimilar to those for meteorites (Data: YDB from Firestone *et al.,* 2007, 2010.

Meteorites from Lodders and Fegley, 1998; Newsom, 1995). They are also geochemically unlike impact-related tektites from the Ivory Coast (Data: Koeberl, 2007), impact-related melt-rocks, or escoria, from Argentina (Data: Schultz *et al.*, 2006), and most Chesapeake Bay tektites (Data: Poag *et al.*, 2004; Koeberl *et al.*, 1988). On the other hand, the values overlap Australasian tektites (Data: Amare and Koeberl, 2006), and Czech Moldavites (Data: Koeberl *et al.*, 1988), indicating a terrestrial origin. Also, SLO values fall within the black-circled area that represents post-Archean upper continental crust (<2.5 Ga), including surface sediments, riverine deposits, shales, mudstones, and clays (Data: Taylor and McClennan, 1985). YDB object compositions are inconsistent with Archean sediments (>2.5 Ga) (Data: Taylor and McClennan, 1985), suggesting that likely source-materials were <2.5 Ga in age.

Chromium-nickel ratios (Figure S10C). This binary diagram compares nickel (Ni) and chromium (Cr) abundances in YDB objects with terrestrial material and meteorites. YDB objects are highly dissimilar to known iron meteorites (blue line), and a few fall in the typical ranges for chondrites (purple line). On the other hand, nearly all are within the range of terrestrial rocks and sediments (green line). (Data: terrestrial values from McDonough, 1998; chondrite data from Lodders *et al.*, 1998; and iron meteorite data from Daode *et al.*, 1996.]

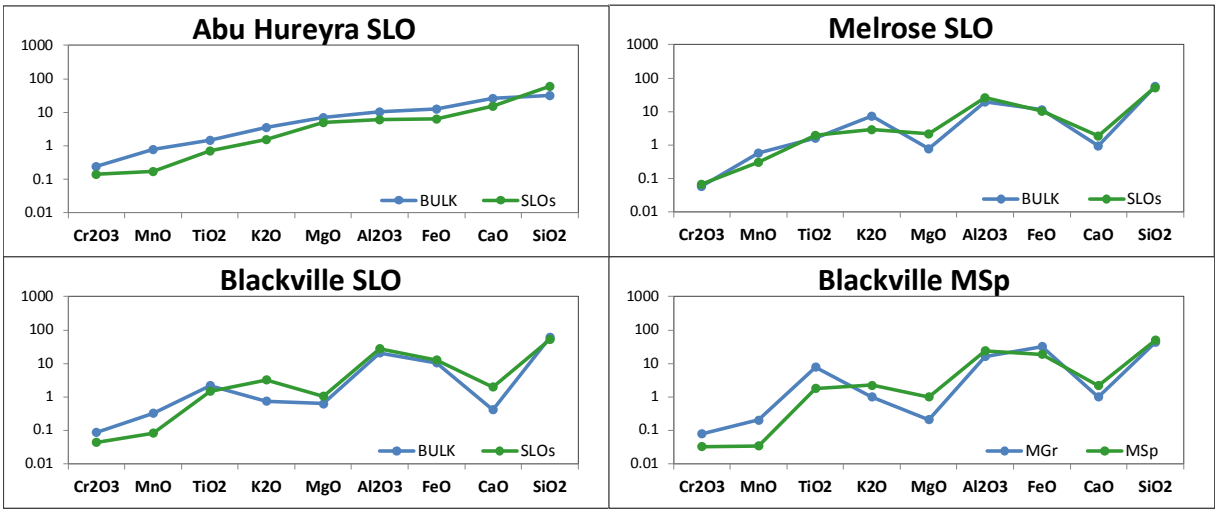

Figure S11. Major Oxides. Percentages of major oxides for Abu Hureyra, Melrose, and Blackville are plotted comparing SLOs (green) with bulk sediment (blue). SLOs analyzed with SEM-EDS compare favorably to bulk sediment analyzed with neutron activation analyses (NAA) and prompt gamma activation analyses (PGAA) (Firestone *et al.*, 2007, 2010) within a range of approximately ±4×. The lower right panel demonstrates that Blackville spherules (MSp, green) compare closely to the site's magnetic grains (MGr, blue) and to SLOs shown in lower left panel. These results suggest that for each site, the SLOs and spherules could have formed from melted local sediment. In addition, the results demonstrate that SLOs and spherules from eastern North America are geochemically similar to each other, but dissimilar to SLOs found at Abu Hureyra in Syria.

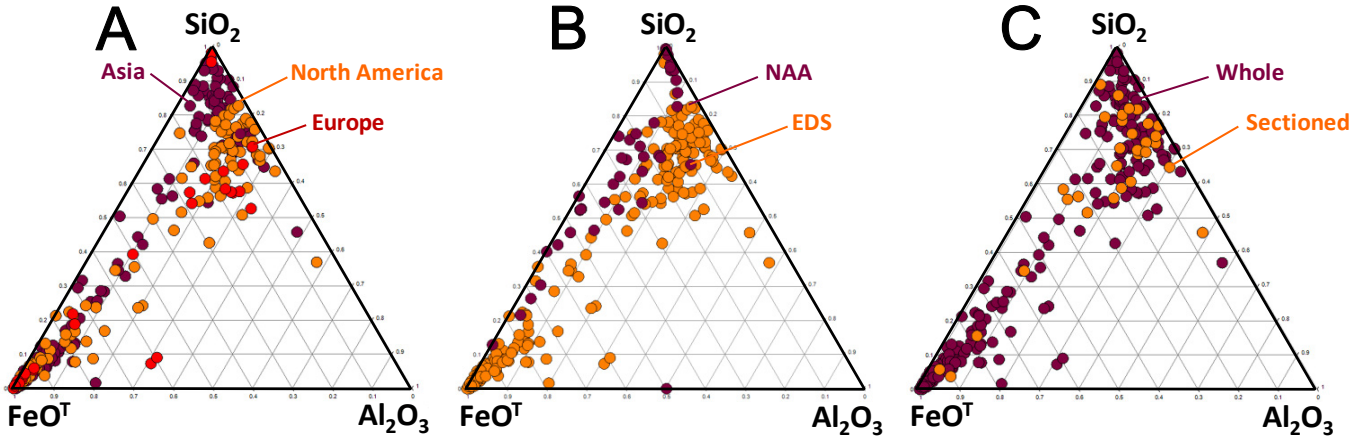

Figure S12. Comparative Analyses of Datasets. A comparison of major elemental percentages (Fe, Al, and Si): **A) Different continents:** YDB objects are indistinguishable by continent. **B) C) EDS vs. NAA;** for six sites (Blackville, Blackwater Draw, Gainey, Lommel, Topper, and Murray Springs), we have neutron activation analysis (NAA) for bulk sediment (YDB from Firestone *et al.,* 2007, 2010), along with elemental analyses using SEM-EDS for YDB objects. The results show no significant difference in composition, suggesting that YDB objects are derived from local sediments. **C) Whole or sectioned YDB objects** are geochemically similar, indicating that the accuracy of analyses appears unaffected by method of preparation.

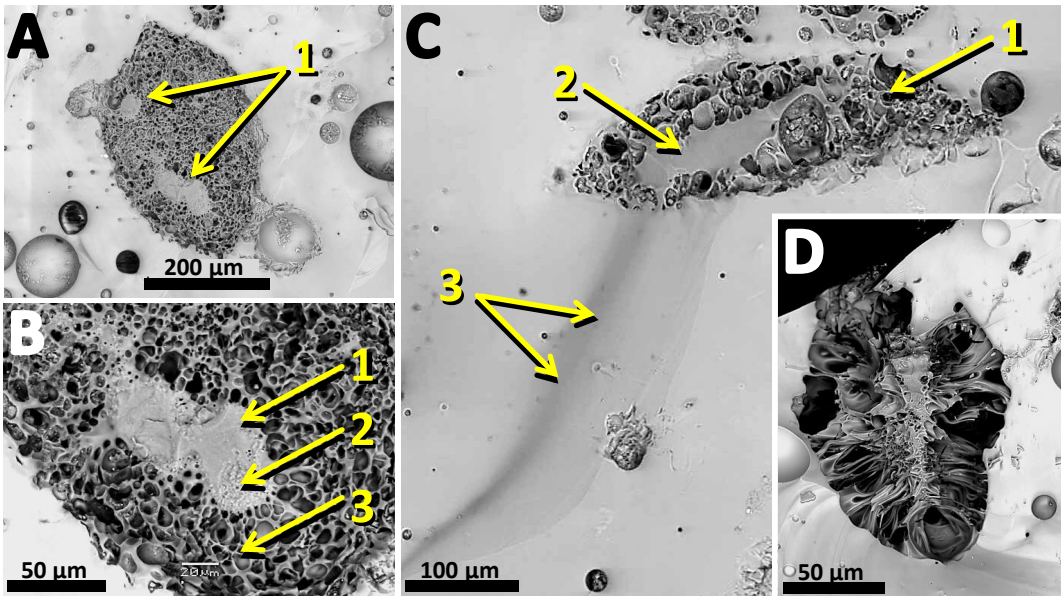

Figure S13. **Melting and evaporation of quartz** in Muong Nong layered tektite glass from the Australasian tektite field. **A)** Residual quartz and non-vesiculated silica (lechatelierite) regions of a boiled quartz grain at #1. **B)** Close-up shows non-vesiculated silica glass at #1, partially melted quartz at #2, and frothy silica glass (boiled quartz) at #3. **C**) Frothy silica glass at #1 with non-vesiculated silica glass core at #2 (SiO_2 = 99 wt%) that has leaked into and formed a long streak within the lighter gray tektite glass matrix at #3 (SiO_2 = 74 wt%). **D)** Completely boiled quartz grain. These four examples suggest minimum temperatures of 2230°C, the boiling point of quartz.

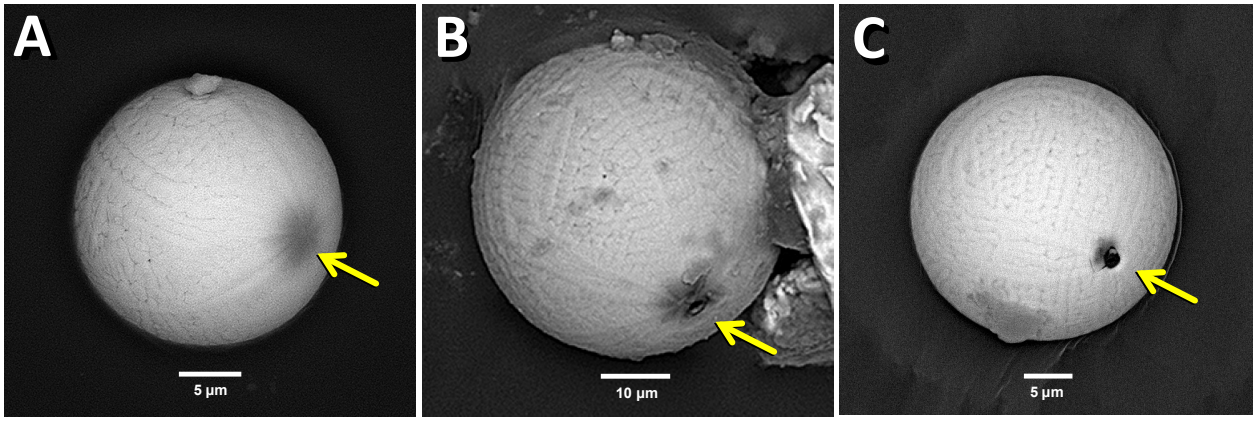

Figure S14. Carbon-rich impactors. A) Blackwater Draw: craterless non-penetrating impact by low-velocity carbon particle onto a magnetic spherule. **B) Kimbel Bay:** moderately-high-velocity impact (<5 km/sec.) by carbon impactor that penetrated a hollow magnetite-rich spherule, creating a raised rim; crater is 2 µm. YDB spherules frequently have large central vesicles for unknown reasons. There is no evidence that the small impacting spherule exited the larger spherule or survived the impact. **C) Blackwater Draw**: another moderately-high-velocity impact by a carbon impactor that penetrated a hollow magnetite-rich spherule, dimpling and penetrating the host material without forming a raised rim; entry hole is 2 µm.

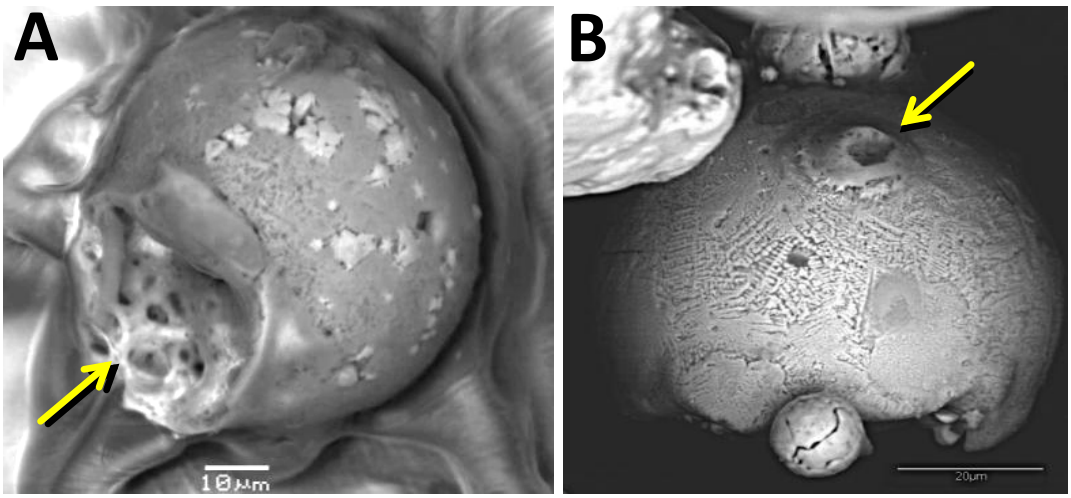

Figure S15. Collisional YDB spherules. A) Lommel. Spherule with hercynite (bright areas) and sillimanite crust (dull, lath-shaped). This spherule exhibits an impact crater (arrow) or a vapor pressure blow-out, revealing aluminosilicate and silica (lechatelierite) interior glasses. **B)** Potential YDB spherule with splash-form impact at arrow that has magnetite quench-crystals on the surface (LeCompte *et al.*, 2010, 2011). Note pit caused by the impact, surrounded by a splash apron with a raised impact rim beyond it, similar to cratering observed by Prasad and Khedekar (2003) and Prasad *et al.* (2010).

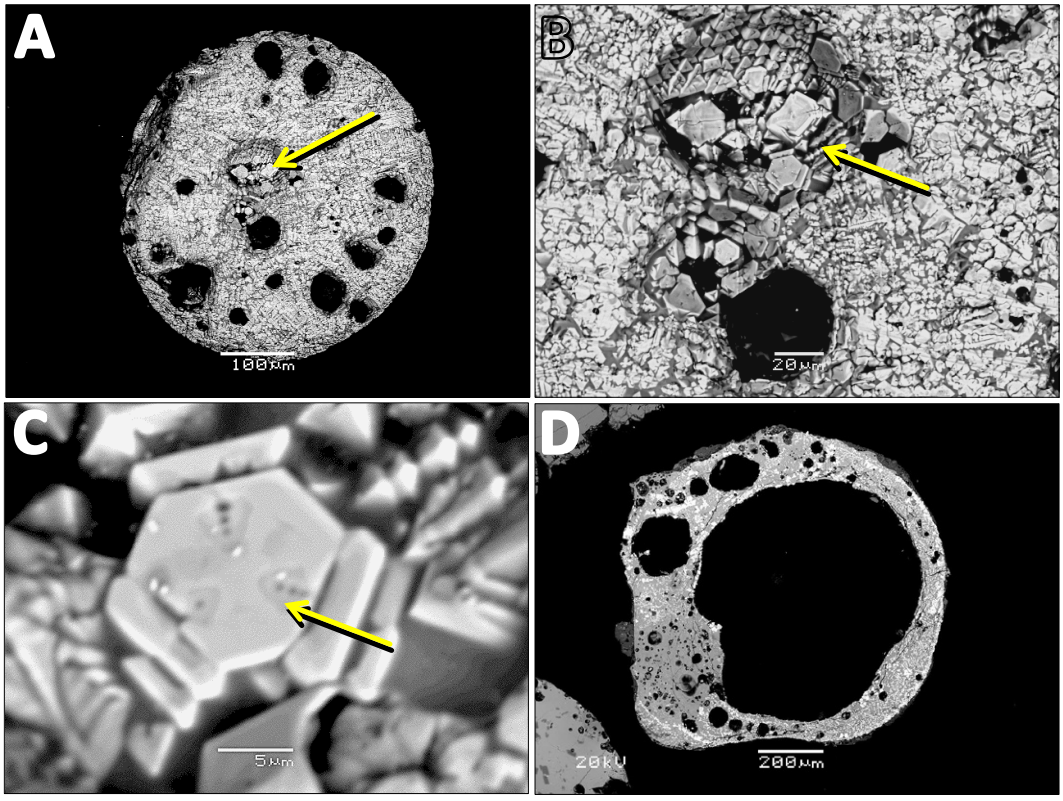

Figure S16. Melrose site, aluminum-rich hematite. A) Spherule displaying vesicles and bubbles with an inclusion comprised of >85 vol.% Al-hematite (arrow) surrounded by aluminosilicate glass. **B) Bubbled interior** of same spherule showing Al-hematite platelets (arrow). **C) Hexagonal platelets** of same spherule, containing trigonal inclusions of Al_2O_3-rich material (arrow). **D) Thin section** of a hollow high temperature spherule with high-density Al-hematite quench crystals and a partial rim of fused clays and quartz. Al_2O_3 contents range from 5.6 to 9.2 wt% for these specimens.

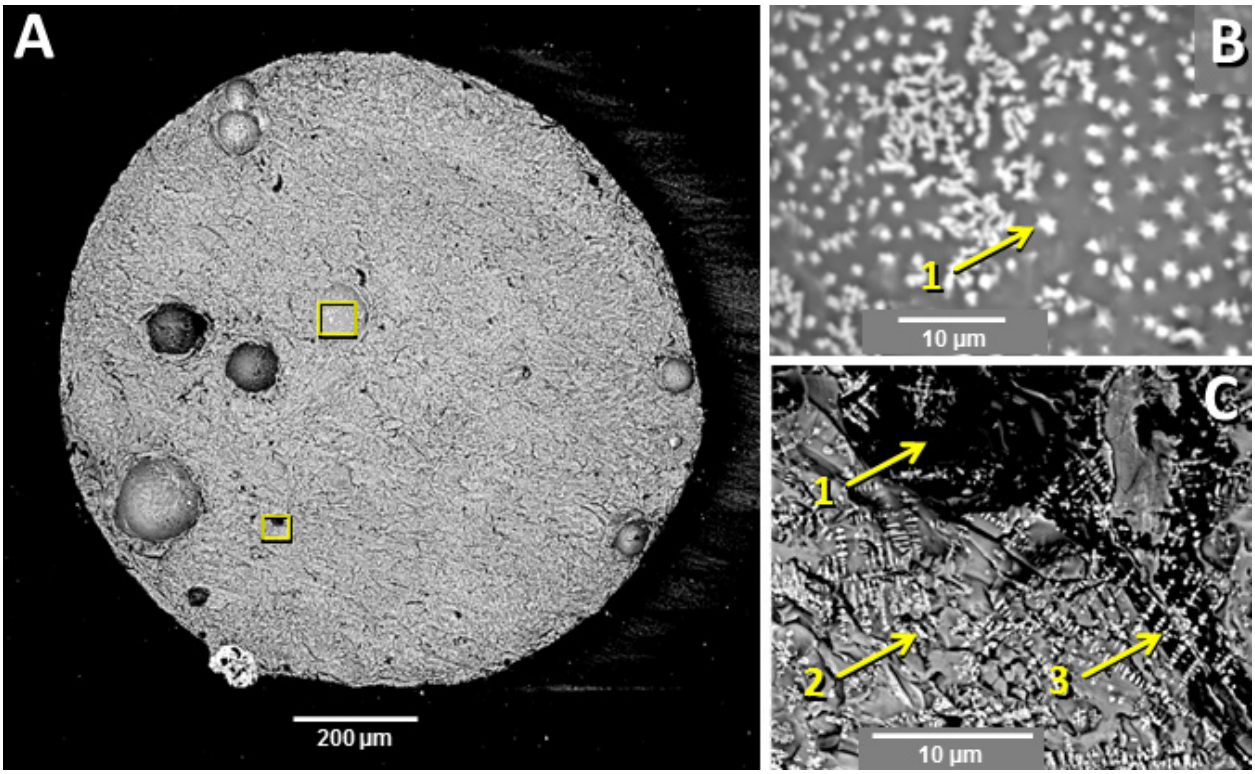

Fig. S17. Blackville. **A)** Overview of aluminosilicate spherule. **B)** Enlargement of upper box in **11A**, showing vapor-deposited magnetite on inside wall of bubble. **C)** Enlargement of lower box in **11A**, showing dark carbon inclusions (no. 1) and dendritic magnetite crystals (no. 2), some intergrown with dark, glassy carbon-rich areas, implying rapid cooling of non-equilibrium melt materials.

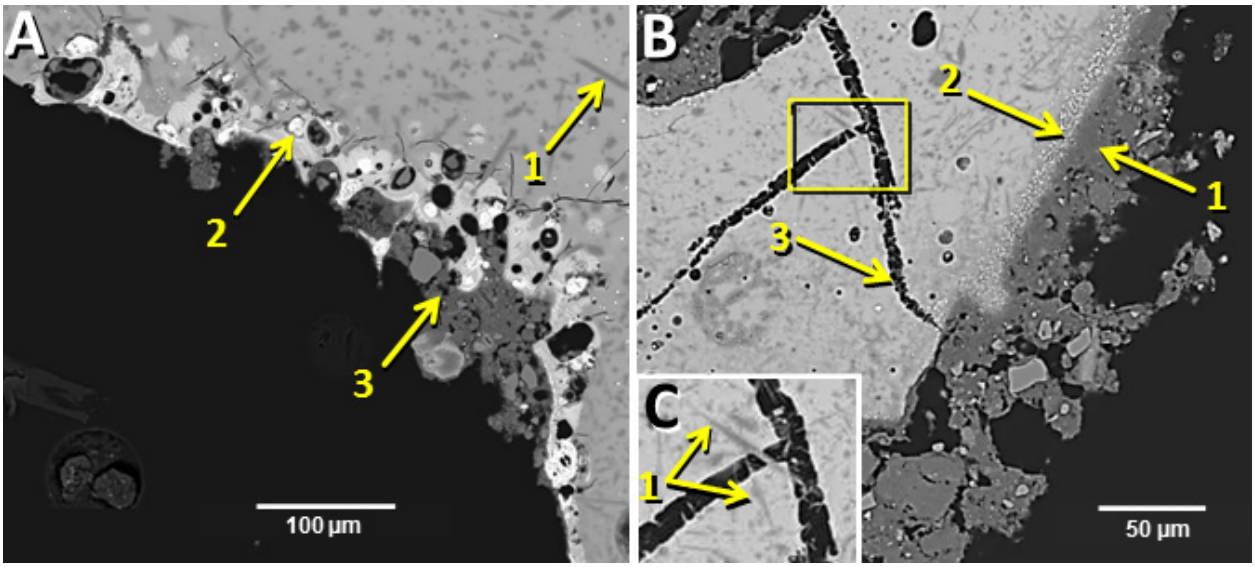

Fig. S18. SEM-BSE image of Blackville SLOs. A) Portion of aluminosilicate glass shard displaying spindle-like mullite quench crystals (no. 1), metallic Fe particles (no. 2), and a reaction rim with fused soil-like material (no. 3). Bright material in rim is quenched magnetite. Soil consists of kaolinite and illite clays, quartz, chlorite, iron oxides, and altered feldspar. **B)** SLO showing a reaction rim composed of soil (no. 1). Bright phase under the rim is hercynite spinel (no. 2); dark veins are glass-like carbon (no. 3). **C)** Inset box from **12B** shows mullite crystals (no. 1) intergrown with carbon-filled areas, indicating high-temperature crystallization.

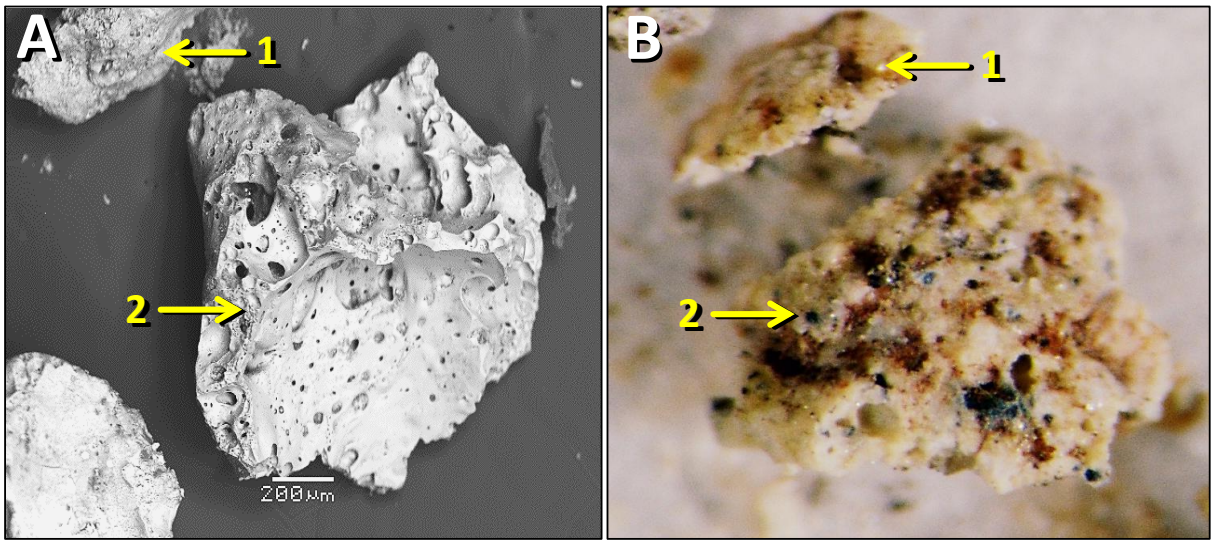

Figure S19. Abu Hureyra. **A) SEM-BSE image** of SLO exhibiting highly vesiculated texture of melted quartz, carbonate, and iron oxides. **B) Light microscope image** of the same grain, slightly rotated.

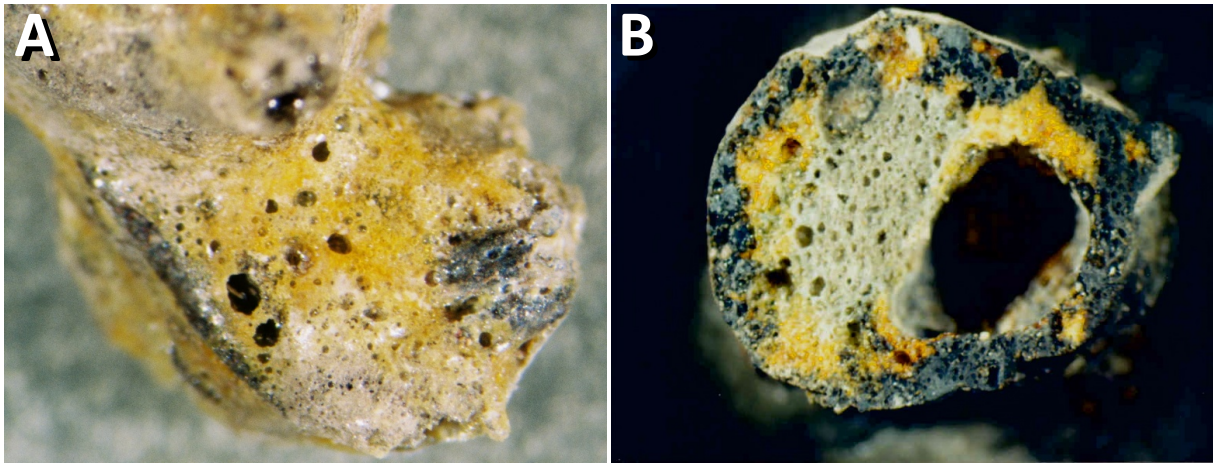

Figure S20. CaO-rich SLOs from the melting of carbonate and silica-rich precursor rocks. **A) Abu Hureyra** SLO; width is 3 mm. Yellow area is CaO-rich (CaO = 35.3 wt%); white to clear is lechatelierite; dark is FeO-rich. **B) Meteor Crater** SLO; width is 5 mm. Yellow is CaO-rich (CaO = 32.5 wt%); clear to gray is lechatelierite; dark is FeO-rich.

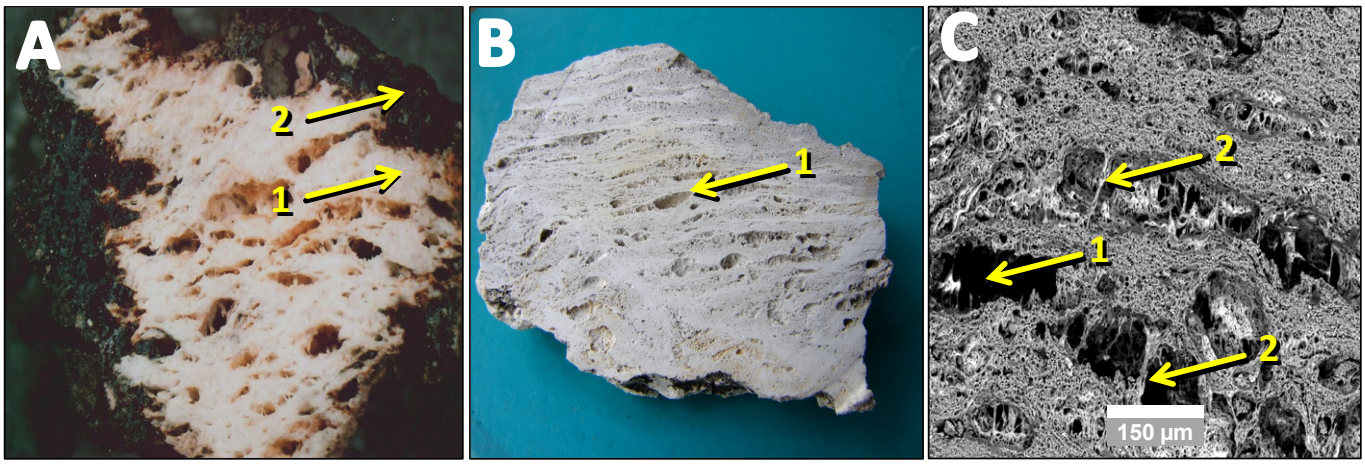

Figure S21. **A) Meteor Crater;** light-colored pumice-like lechatelierite (#1) covered by a dark Ca-rich carbonate melt (#2) that penetrates into lechatelierite voids (width of the impactite = 12 mm). **B**) **Haughton crater;** pumice-like lechatelierite (width = 72 mm) with pulled-apart texture (#1). **C**) **SEM-BSE image** of enlarged portion of **19B** that shows the high porosity level, pulled-apart texture (#1) and vesiculated taffy-like SiO_2 melt stringers (#2).

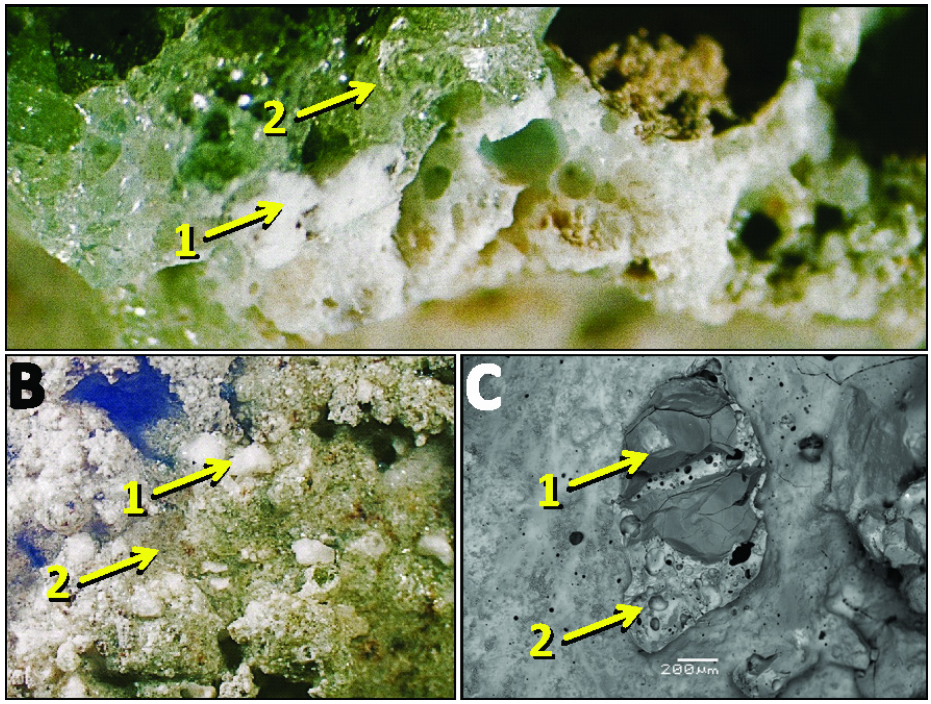

Fig. S22. Trinity: images of puddled trinitite fallback melt that shows melted to partially melted surface arkosic sand minerals. **A)** Edge-on image of trinitite green glass (width, 17mm); white is melted K-feldspar (no. 1); clear glass is melted quartz or lechatelierite (no. 2). **B)** Green trinitite shows embedded, melted K-feldspar (white, no. 1), and partially to fully melted quartz (no. 2) (width, 8 mm). The implied interface temperature between trinitite melt and arkosic sand is >1730ºC. **C)** SEM-BSE image showing unmelted quartz grain (no. 1) set in melted K-feldspar (no. 2) surrounded by trinitite. Implied temperature is >1200ºC, the melting temperature of K-feldspar, and <1730ºC, the melting temperature of quartz.

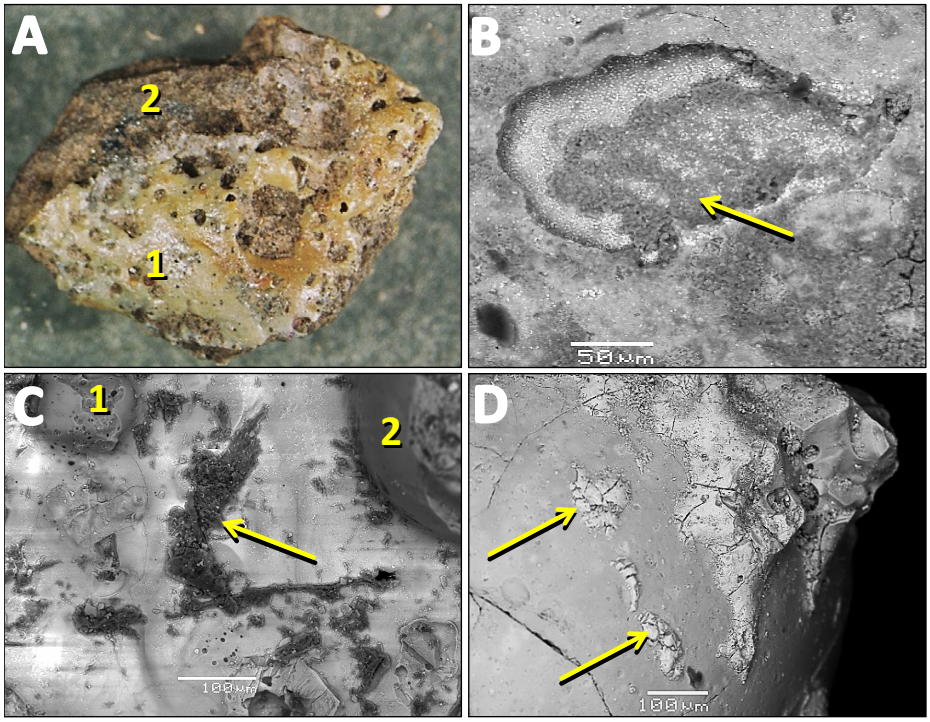

Figure S23. Molten splash-forms. A) Melrose. Fe-rich aluminosilicate melt splash (#1) on shale (#2); width = 3 mm. **B) Meteor Crater.** Molten splash on large SLO that contains tiny magnetite quench crystals and a mass of carbon in the interior (dark gray at arrow). **C) Trinitite** surface with splash-form carbon (dark gray at arrow) and two accreted spherules (#1, #2), formed through nuclear detonation. **D) Trinitite**. Clumpy melt splash on spherule with small puddles of lechatelierite (arrows), formed through nuclear detonation.

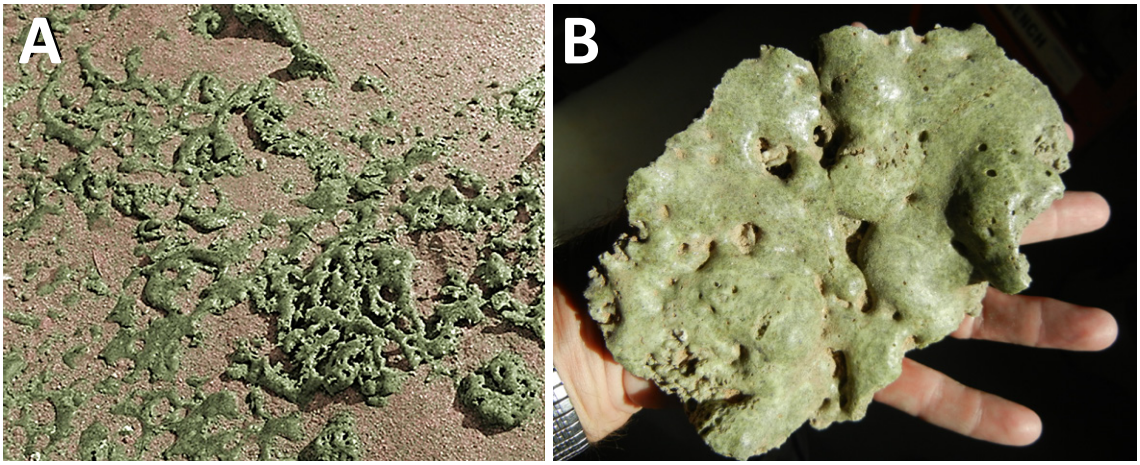

Figure S24. Pooled trinitite. A) Colorized photo of *in situ* trinitite on ground after the nuclear detonation. Width of view is about 50 cm. **B)** Large piece dubbed the "Green Monster" is about 18 cm long. Visible side was facing up on the ground.

NUCLEAR AND ET AIRBURSTS

The thousands of people who worked on the Manhattan project and tested the first atomic bomb at the Trinity Site probably did not anticipate that their efforts would later serve as a real-time experiment for the study of catastrophic cosmic aerial impact bursts. The ET impact events proposed to have produced Libyan Desert Glass (LDG), the Australasian tektites, Dakhleh glass, and Tunguska glass are probable aerial bursts. Wasson (1998, 2003) investigated the characteristics of some of these glasses, the Australasian tektites and LDG glass, and found these glasses to be inconsistent with crater-forming impacts, and yet, as we have also found, are very similar to the formation and characteristics of trinitites**.** The most significant are: A) Layered glasses that formed as pools of melt from the raining of droplets from the hot impact plume. B) These layered glasses melted at very high temperatures and are nearly devoid of unmelted materials. The temperature of the glasses was >2000°C and melting was evenly distributed throughout, in contrast to heterogeneous melt breccia and suevite-like products from crater-forming impacts that sustained lower initial temperatures (Wasson and Moore, 1998). C) Tektites, LDG, and trinitites were produced from surface sediment precursors, not deep-seated rocks.

Although Dakhleh, Tunguska, and the YDB sites lack large-scale layered glasses, these inferred aerial bursts did produce splash or spin-form glasses (spherules, teardrop, dumbbell, etc.) similar to tektites and trinitites, all of which formed by spinning and cooling in an impact plume (Elkins-Tanton *et al.,* 2003). Whether or not massive layered glasses are produced depends on several factors, the most important of which is the burst altitude (Vasilyev, 1998; Boslough and Crawford, 2007). The most intense heating would come from a blast that is very near the Earth's surface, e.g., the Trinity detonation at 20 kt of energy 30 m above the ground. In contrast, the air burst energy for Tunguska was orders of magnitude greater, but the burst altitude was much higher at 5-10 km (Svetsov, 2006), thus the thermal damage was significantly less, although Tunguska tektites have been reported (Kirova *et al.*, 1966). A comparison of other plume products from these impact events is given in **SI Table 1.**

HEATING: Impact vs. Atomic

Nuclear airbursts heat the atmosphere and surface soils by kinetic energy, as well as by intense gamma and beta nuclear radiation. This contrasts with a kinetic airburst during a cosmic impact, which mostly heats by thermal to micro-wave radiation. A breakdown of the approximate energy released by fission in a nuclear detonation is as follows:

MeV kinetic energy of fission fragments	165
Instantaneous gamma rays	7
Kinetic energy of neutrons	5
Beta particles from product decay	7
Gamma rays from product decay	6
Neutrinos from product decay	10
TOTAL (MeV):	200

For both types of events, the post-heating processes are similar (e.g., lofting, collisions, and entrainment), because, regardless of whether a detonation is the result of chemical, nuclear, or kinetic airburst, the thermal effects are much the same. During all types of airbursts, thermal radiation is released and a flash-heating event of 1000's of degrees C is generated, followed by an overpressure wave and finally an underpressure wave.

Another major difference among the two types of events is that nuclear detonations are static, whereas the aerial burst from an impacting body is dynamic with momentum and delivers the heat to the surface at high velocity. The radiation heat that fluxes to the ground increases with increasing velocity of the impactor. So, in comparing an atomic detonation with a cosmic airburst with equivalent energy in terms of TNT, a cosmic airburst delivers a greater thermal radiation flux to the surface and, hence, has greater melting efficiency. However, it does not change the melting and quenching effects on the melted surface soil, i.e., glass formed from temperatures >2000°C will have the

same characteristics regardless of the mechanism.

FULGURITES

Lechatelierite is present in two types of lightning-generated melt material. 1) Subsurface fulgurites form when cloud-to-ground lightning melts mostly unconsolidated sediment. 2) Exogenic fulgurites, which are much rarer, form when very high-energy lightning melts unconsolidated sediment or rocks, such as on mountaintops (French, 1998; Wasilewski P and Kletetschka G, 1999; Carter, *et al.* 2010; Walter, 2011)

SUBSURFACE FULGURITES are hollow, glassy tubes usually up to 1-2 cm in diameter with walls several millimeters thick (Sponholz *et al.* 1993, 2004), but rare ones range up to approximately 15 cm in diameter and may form branches of melt material extending several meters underground. For these fulgurites, the lightning typically affects only a few cm of ground around the subsurface fulgurite (Walter, 2011). The inner surface of the tube is highly polished and comprised of fully melted grains that have flowed together completely to form vesicular lechatelierite. From the smooth inside surface outward, the fulgurite displays a gradation from a) fully melted highly reflective glass to b) partially melted grains and glass to c) unmelted grains fused to glass forming a rough, sandy outer surface (Sponholz *et al.* 1993, 2004). This morphology is distinctive and easily recognized.

EXOGENIC FULGURITES appear as vesicular glassy spherules and droplets that are usually less that 5 cm in diameter. They are formed by the most energetic of lightning strikes that create a subsurface fulgurite and then, eject melted glass up to a meter away (Walter, 2011).

GEOCHEMISTRY. Analyses of fulgurites indicate that they are comprised of typical surficial sediments rapidly heated to >2300°C, then rapidly cooled, resulting in reduced (oxygen-deficient) glass (Sheffer *et al.* 2006). Most fulgurites are enriched in SiO_2 (>70 wt%) and depleted in FeO (<8 wt%) (Walter, 2011; Carter *et al.* 2010). Because fulgurites form from terrestrial sediments and rocks, they closely resemble melted material from cosmic impact events and nuclear airbursts (Sheffer *et al.* 2006). However, there are recognizable differences, as follows:

1) Collisional Damage. Fulgurites form in high-temperature, lower-energy events, which eject low-velocity melted particles that are incapable of causing collisional damage to other particles (Prasad and Khedekar, 2003). This is unlike high-velocity cosmic impacts/airbursts and nuclear detonations that can cause considerable collisional damage.

2) Ultrastructure. Subsurface fulgurites, the most common variety, are easily recognized when encountered in a sedimentary profile because of their tube-like shape. Their walls tend to be only several millimeters thick, and so, they can break into smaller pieces. However, they are still recognizable because their inner surfaces typically are shiny and their outer surfaces are rough and coated with fused sand grains. YDB SLOs do not display this morphology.

3) Lateral Distribution of Glass (SLOs). At Abu Hureyra, we sampled about 4.5 m away in the stratum above the YDB layer and observed SLOs in both places. At Blackville, two samples approximately 10 m apart displayed glass as SLOs. At Melrose, two samples 28 m apart displayed melted glass. The results from the three sites indicate that the SLOS are not limited to just one small area of each site, but rather, range from 4.5 to 28 m apart. By comparison, exogenic fulgurites are not reported beyond a 1-m radius of a subsurface fulgurite (Walter, 2011). Thus, the YDB SLOs are not limited to just one confined area of each site, as would be the case with a lightning strike. This suggests that the observed glass from these three sites was not produced by lightning strikes.

4) Rarity of Glass in Sedimentary Column. Of the 18 sites investigated, some spanning a range of >16,000 years, we did not observe any fulgurites or fragments of them. The only glassy material (SLOs) that we found was morphologically different and displayed large peaks in the 12.9-ka YDB layer with low quantities in adjacent layers. Strata that were remote from the YDB contained no or few pieces of impact-type glass or SLOs.

Even though fulgurites are accepted to be rare in sedimentary profiles, it has been proposed by Pigati *et al.* (2010) that they and other YDB-like proxies, such as spherules and iridium, might become concentrated on deflational surfaces or under the wetland-related black layers or mats. One could speculate that this might occur in relation to extreme weather conditions at the onset of Younger Dryas cooling episode. Eight of our sites have such black layers (Arlington Canyon, CA; Blackwater Draw, NM; Chobot, AB, Canada; Lake Cuitzeo, Mexico; Gainey, MI; Murray Springs, AZ; Sheriden Cave, OH; and Talega, CA). Of those eight sites, only one (Murray Springs) displays glass, but it is clearly not fulguritic, according to Fayek *et al.* (2012). Also, at Murray Springs, we sampled several stratigraphically separated black mat layers that were younger than the YDB-related mat layer, and none of those contained fulgurites, glass, or spherules. Four other sites have charcoal-related black layers (Lingen, Germany; Lommel, Belgium; Ommen, Netherlands; and Abu Hureyra, Syria), and of those, only Abu Hureyra displays glass as SLOs that are morphologically unlike fulgurites. Thus, at these twelve sites with black layers, not one fulgurite tube or fragment was observed in the YDB, or in strata above it and below it. These observations indicate that fulgurites are not common at our collection sites and suggest that they are not concentrated by black mat layers.

In conclusion, high-temperature lechatelierite melt-glass is only known to result from lightning strikes, atomic detonations, and cosmic impacts. The available evidence does not support an origin of YDB glass by lightning and instead, supports an impact origin.

TABLES

SI Table 1. Comparison of high-temperature proxies from various sources: YDB, Trinity detonation (TRIN), Meteor Crater (METC), Australasian tektite field (AUST), and Tunguska (TUNG). The range of proxies reported is nearly identical for all events. [References: B=Bunch *et al.* (2012); C=Chao *et al.* (1962); F=Florenskiy *et al.* (1963); K=Kirova *et al.* (1966); P=Prasad *et al.* (2003); and Z=Zbik (1984).]

	YDB	TRIN	METC	AUST	TUNG
Magnetic spherules	B	B	B*	C	F
Silicate spherules	B	B	B	P	K
Melted glass (SLOs)	B	B	B	B	K
Lechatelierite	B	B	B	B	K
Micro-craters	B	B	B	P	Z
Melt drapings/splash	B	B	B	P	Z
Spherule accretions	B	B	B	P	Z
Carbon-to-Si accretions	B	B	B	n/a	n/a

Note: *Rich in Ni-Fe from impactor. Rich in Fe from target.
"n/a" = not tested

SI Table 2. Site information and dates. Age-depth models were established for Abu Hureyra using 13 AMS ^{14}C dates and for Blackville and Melrose using OSL dating. Dates for the three sites were graphed using linear interpolation (**SI Figs. 2, 4, 5)**, and in each case, the intersection of the YD onset at 12.9 ka coincided the depth of the peaks in YDB proxies. The column "YDB?" indicates the dates closest to the YDB layer.

Site	Lat/Lon	Elev. (m)	Lab	Depth	Level	RCYBP	±	Cal BP	±	YDB?	Type	Material	Reference
Abu Hureyra	35.8667°N	310	OxA-170	285.33	405	10600	200	12430	270	--	AMS	Charred grain	Moore, et al. 2000
	38.4000°E	--	OxA-407	285.13	419	10050	180	11680	320	--	AMS	Charred bone	Moore, et al. 2000
	--	--	OxA-386	285.12	420	10800	160	12780	140	--	AMS	Charred grain	Moore, et al. 2000
	--	--	OxA-473	284.95	425	10000	170	11610	290	--	AMS	Charred bone	Moore, et al. 2000
	--	--	OxA-397	284.91	430	10420	140	12310	240	--	AMS	Charred grain	Moore, et al. 2000
	--	--	OxA-434	284.91	430	10490	150	12370	230	--	AMS	Charred bone	Moore, et al. 2000
	--	--	OxA-171	284.72	457	10600	200	12430	270	--	AMS	Charred grain	Moore, et al. 2000
	--	--	UCIAMS-105429	284.70	445	11070	40	12932	176	**Yes**	AMS	Charcoal	This paper
	--	--	BM-1718R	284.67	447	11140	140	13040	150	**Yes**	AMS	Charcoal	Moore, et al. 2000
	--	--	OxA-430	284.56	460	11020	150	12940	130	**Yes**	AMS	Charred bone	Moore, et al. 2000
	--	--	OxA-172	284.29	470	10900	200	12870	160	**Yes**	AMS	Charred seed	Moore, et al. 2000
	--	--	OxA-468	284.29	470	11090	150	13000	160	**Yes**	AMS	Charred bone	Moore, et al. 2000
	--	--	OxA-883	284.29	470	11450	300	13370	300	--	AMS	Charred grain	Moore, et al. 2000
Blackville	33.361545°N	98	LB862	107	--	--	--	11500	1030	--	OSL	Quartz grains	This paper*
	81.304348°W	--	LB861	152	--	--	--	18540	1680	--	OSL	Quartz grains	This paper*
	--	--	LB859	183	--	--	--	12960	1190	**Yes**	OSL	Quartz grains	This paper*
Melrose	41.925350°N	419	LB860a	28	--	--	--	16400	1600	**Yes**	OSL	Quartz grains	This paper*
	75.510066°W	--	--	--	--	--	--	--	--	--	--	--	--

*OSL Dating by: IIRMES laboratory, California State University Long Beach.

SI Table 3. Abundances of Proxies. This table shows midpoint depth in cm relative to YDB, thickness of layers, magnetic grain (MGr) abundances in g/kg, spherules (MSp) in #/kg, and SLOs in g/kg.

Abu Hureyra, SYR					Blackville, SC					Melrose, PA				
Cm	Thick	MGr	MSp	SLO	Cm	Thick	MGr	MSp	SLO	Cm	Thick	MGr	MSp	SLO
290	5.00	--	--	0.04	76	15	1.20	190	0.00	9	10	6.96	310	0.76
78	5.00	129	0	0.23	61	15	1.10	115	0.01	0	8	2.71	3110	0.80
0	5.00	74	595	15.76	46	15	1.10	90	0.00	-6	5	4.18	1190	0.05
-12	5.00	182	0	0.02	30	15	0.10	70	0.04	-14	10	11.06	70	0
					15	15	1.30	205	0.03	-24	10	0.66	210	0
					0	15	1.30	525	0.06					
					-15	15	1.70	0	0.00					
					-30	15	4.00	0	0.00					
					-46	15	4.40	2	0.00					
					-61	15	1.40	0	0.00					
					-76	15	1.40	5	0.00					

SI Table 4. Average oxide abundances for SLOs, spherules, and bulk sediment in wt% by site. Crustal abundances are also listed. Some bulk sediment values from Firestone *et al.* (2007, 2010).

Type	SITE	Al_2O_3	CaO	Cr_2O_3	FeO^T	K_2O	MgO	MnO	Na_2O	NiO	P_2O_5	SiO_2	SO_3	TiO_2
SLOs	Abu Hureyra	5.97	15.17	0.14	6.30	1.53	5.06	0.17	1.17	0.05	3.76	59.44	0.54	0.69
	Blackville	27.66	1.92	0.04	12.56	3.13	1.02	0.08	0.51	0.15	0.25	51.13	0.11	1.45
	Melrose	25.92	1.90	0.07	10.13	2.87	2.12	0.31	0.83	0.09	0.30	53.16	0.4	1.92
	SLOs AVG:	**19.85**	**6.33**	**0.08**	**9.66**	**2.51**	**2.73**	**0.18**	**0.84**	**0.10**	**1.44**	**54.58**	**0.35**	**1.35**
	Crustal Values	**15.42**	**4.00**	**0.01**	**5.34**	**3.10**	**2.77**	**0.08**	**3.33**	**0.00**	**0.17**	**65.16**	**0.00**	**0.63**
Spherules	Abu Hureyra	8.97	10.06	0.03	11.51	2.58	4.85	0.29	1.56	0.06	1.55	56.94	0.93	0.66
	Blackville	22.85	1.80	0.00	21.39	2.44	1.05	0.04	0.24	0.05	0.19	49.00	0.00	0.96
	Melrose	21.06	1.50	0.12	32.00	1.70	0.63	0.11	0.86	0.11	0.49	39.80	0.39	1.24
	Spher. AVG:	**17.63**	**4.45**	**0.05**	**21.63**	**2.24**	**2.18**	**0.15**	**0.89**	**0.07**	**0.74**	**48.58**	**0.44**	**0.95**
	Crustal Values	**15.42**	**4.00**	**0.01**	**5.34**	**3.10**	**2.77**	**0.08**	**3.33**	**0.00**	**0.17**	**65.16**	**0.00**	**0.63**
Bulk Sed	Abu Hureyra	10.51	25.70	0.24	12.42	3.49	6.88	0.77	1.00	0.02	2.02	31.37	4.10	1.48
	Blackville	20.61	0.41	0.09	10.22	0.74	0.00	0.32	0.00	0.00	2.26	61.27	1.88	2.20
	Melrose	19.13	0.93	0.06	11.36	7.23	0.79	0.59	0.08	0.00	1.12	56.28	0.80	1.65
	Bulk AVG:	**17.63**	**4.45**	**0.05**	**21.63**	**2.24**	**2.18**	**0.15**	**0.89**	**0.07**	**0.74**	**48.58**	**0.44**	**0.95**
	Crustal Values	**15.42**	**4.00**	**0.01**	**5.34**	**3.10**	**2.77**	**0.08**	**3.33**	**0.00**	**0.17**	**65.16**	**0.00**	**0.63**

SI Table 5. DATA SOURCES for TERNARY DIAGRAMS of cosmic, anthropogenic, volcanic, and impact-related materials. Materials are shown by type, sampling location, number of sites, number of analyses per site, and references. Note: "Micromet." equals "micrometeorites."

TYPE	LOCATION or TYPE	SITES	ANAL.	REFERENCE
ANTHROPOGENIC				
Spherules	USA	1	42	This paper
Fly ash	AUS	27	6	Provis, 2009
	AUS		14	Ward, 2006
	BUL		3	Shoumkova, 2006
	CAN, JAP, USA, UK, FRA		5	Gikunoo, 2004
	CHN		2	Gao, 2004
	CHN		3	Yijin, 2004
	CZE		1	Sulc, 2009
	EST		1	Marini, 2009
	IND		11	Chandra, 2009
	IND		9	Mandal, 2006
	IND		25	Natarajan, 2007
	IND		2	Sivakumar, 2009
	ISR, CHN, USA, GER, JOR		10	Oymael, 2007
	JAP, PHL, THA		6	Yamada, 2001
	NLD		1	Nugteren, 2009
	NZL, AUS		2	Keyte, 2004
	POL		12	Jablonska, 2003
	POL		10	Uscinowicz, 2009
	S.AFR		1	Muriithi, 2009
	SPN		13	Acosta, 1997
	SPN, NLD, GRE, ITA		23	Towler, 2002
	TWN		1	Wang, 2003
	UK		5	Snelson, 2007
	USA		7	Bhatty, 2001
	USA		2	Giere, 2003
	USA		19	Jewell, 2009
	USA		5	McKeen, 1998
	USA		13	White, 2005
	USA, TUR, POL, PRT, CHN, ITA, SPN, EGY, IND		13	Rawlings, 2006
	TOTAL ANTHROPO:	**28**	**267**	
VOLCANIC				
Glass	Atlantic, Pacific, Indian, Carib.	193	10026	Melson, 2002
Spherules	Pacific	2	57	Melson, 1988
	Pacific		119	Vallier, 1977
Tephra	Andean volcanoes (3)	10	19	Kilian, 2003
	Crater Lake		21	Bruggman, 1993
	Glacier Peak, St. Helens		8	Carrara, 1992
	Glacier Peak, St. Helens		124	Hallett, 2001
	Iceland		31	Wastegard, 2001
	Laacher See		17	Worner, 1984
	Minoan tephra		183	Weiss, 1993
	St. Helens		2	Fiacco, 1993
	Toba; Pacific Ocean		24	Mascarenhas, 2006
	TOTAL VOLCANIC:	**205**	**10631**	

TYPE	LOCATION or TYPE	SITES	ANAL.	REFERENCE
COSMIC				
Spherules	Antarctica	3	20	Engrand, 1999
	Antarctica		71	Genge, 1997
	Antarctica		20	Genge, 1998
	Antarctica		14	Rochette, 2008
	Antarctica		279	Taylor, 2000,2002
	Antarctica		14	Rochette, 2008
	Atlantic Ocean		45	Dekov, 2007
	Greenland		8	Maurette, 1986
Micromet.	Antarctica	80	21	Engrand, 1999
	Antarctica		86	Genge, 1997
	Antarctica		78	Kurat, 1994
	Meteorites, misc.		77	Genge, 1999
	TOTAL COSMIC:	**83**	**733**	
IMPACTS				
Ejecta	KPg	2	15	Bauluz, 2004
	KPg		12	Koeberl, 1992
	Rio Cuarto		3	Bland, 2002
Spherules	Lonar Crater, IND	3	40	Misra, 2009
	Nuussuaq, Greenland		79	Jones, 2005
	Tunguska, Russia		13	Dolgov, 1973
	Tunguska, Russia		4	Glass, 1969
Tektites	Australasian tektite field	7	6	Amare, 2006
	Australasian tektite field		2	Chalmers,1976
	Australasian tektite field		47	Folco, 2008
	Australasian tektite field		48	Glass, 1990
	Australasian tektite field		47	Glass, 2004
	Australasian tektite field		16	Glass, 2006
	Australasian tektite field		19	Koeberl, 1992
	Australasian tektite field		30	Lee, 2004
	Australasian tektite field		11	Son, 2005
	Bahia Blanca, Argentina		2	Schultz, 2004
	Chesapeake Bay crater		2	Glass, 1990
	Chesapeake Bay crater		28	Glass, 1998
	Chesapeake Bay crater		130	Kelly, 2004
	Chesapeake Bay crater		16	Koeberl, 1998
	Chesapeake Bay crater		7	Koeberl, 2001
	Chesapeake Bay crater		46	McHugh, 1996
	Chesapeake Bay crater		18	McHugh, 1998
	Chesapeake Bay crater		7	Povenmire, 1994
	Chesapeake Bay crater		3	Povenmire, 1997
	Darwin glass		18	Koeberl, 1990
	Lake Botsumtwi crater		1	Glass, 1990
	Lake Botsumtwi crater		5	Koeberl, 2006
	Lake Botsumtwi crater		194	Koeberl, 2007
	Lake Botsumtwi crater		30	Luetke, 2008
	Ries crater--moldavites		1	Glass, 1990
	Ries crater--moldavites		118	Trnka, 2002
	Zhamanshin crater		4	Zolensky, 1991
	TOTAL IMPACT:	**12**	**1018**	

REFERENCES

Acosta A, Aineto M, Iglesias I, Romero I, Rincon JM. (2001) Physico-chemical characterization of slag waste coming from IGCC thermal power plant. *Mater Lett,* 50: 246-250.

Amare K and Koeberl C. (2006) Variation of chemical composition in Australasian tektites from different localities in Vietnam. *Meteoritics & Planetary Science* 41, Nr 1, 107–123.

Baker DW, Miranda PJ, Gibbs KE. (2008) Montana Evidence for Extra-Terrestrial Impact Event That Caused Ice-Age Mammal Die-Off. American Geophysical Union, Spring Meeting 2008, abstract #P41A-05.

Bauluz B, Peacor DR, and Hollis CJ.(2004) TEM study of meteorite impact glass at New Zealand Cretaceous-Tertiary sites: evidence for multiple impacts or differentiation during global circulation? *Earth and Planetary Science Letters* 219, 209-219.

Berg TM, *et al.* (1980) Geologic map of Pennsylvania: Pennsylvania Geological Survey, 4th ser., Map 1, 2nd ed., 3 sheets, scale 1:250,000.

Bhatty JI, Gadja J, Miller FM. (2001) Commercialization of High-Carbon Fly Ash in Cement Manufacture; Report No. 00-1/3 1A-1; Illinois Clean Coal Institute: Canterville, IL.

Bland PA, *et al.* (2002) A Possible Tektite Strewn Field in the Argentinian Pampa. *Science* 296, 1109.

Boslough MBE and Crawford DA (2007) Low altitude airbursts and the impact threat. Proc. Hypervelocity Imp. Sym.

Bruggman PE, Bacon CR, Mee JS, Pribble ST, Siems DF. (1993) Chemical Analyses of pre-Mazama Silicic Volcanic Rocks, Inclusions, and Glass Separates, Crater Lake, Oregon. USGS. Open-file Report 93-314.

Carrara PE and Trimble DA. (1992) A Glacier Peak and Mount Saint Helens J volcanic ash couplet and the timing of deglaciation in the Colville Valley area, Washington: *Canadian Journal of Earth Sciences*, v. 29, no. 11, p. 2397-2405.

Carter EA, Hargreaves MD, Kee TP, Pasek MA, Edwards HGM. (2010) A Raman spectroscopic study of a fulgurite. *Phil. Trans. R. Soc. A*, 368, 3087-3097.

Casson MA and Feathers JK. (2001) The Application of Luminescence Dating to Cultural Resource Management. Society for American Archaeology, New Orleans, LA.

Chalmers RO, Henderson EP, Mason B. (1976) Occurrence, Distribution, and Age of Australian Tektites. *Smithsonian Contributions To The Earth Sciences,* Number 17.

Chandra A, Kumar S, and Kumar S. (2004) Investigations on fly ash Resistivity of varieties of Coals used in Indian power plants. Proceeding, 9th International Conference on Electrostatic Precipitation, Mpumalanga, South Africa B-05.

Chao ECT, Adler I, Dwornik EJ, Littler J. (1962) Metallic spherules in tektites from Isabella, the Philippine Islands. *Science* 135, 97–98.

Colgan PM, Mickelson DM, & Cutler PM. (2003) Ice-Marginal Terrestrial Landsystems: Southern Laurentide Ice Sheet, in Evans, D.A. and Rea, B.R., (eds.), *Glacial Landsystems*, Edwin Arnold, London, 111-142.

Daode W and Yongheng C. (1996) The chemical compositions of Antarctic iron meteorites and their classification. *Advances in Polar Science* 1996, 7(1) 41-49.

Dekov VM, *et al.* (2007) Cosmic spherules from metalliferous sediments:A long journey to the seafloor. *N. Jb. Miner. Abh.,* Vol.183/3, p. 269–282.

Dolgov YA, Vassil'ev AN, Shugurova NA, Lavrent'ev YG, L'vov YA. (1973) The composition of the microscopic spherules from the fallsite of the Tunguska meteorite. *Meteoritika*, 2, 147-149.

Elkins-Tanton LT, Aussillous P, Bico J, Quere D, and Bush JWM. (2003) A laboratory model of splash-form tektites. Meteoritics & Planetary Science 38, Nr 9, 1331–1340.

Engrand C, Deloule E, Robert F, Maurette M, Kurat G. (1999) Extraterrestrial water in micrometeorites and cosmic spherules from Antarctica: An ion microprobe study. *Meteoritics & Planetary Science* 34, 773-786.

Fayek M, Anovitz LM, Allard LF, Hull S, Haynes, CV Jr. (2012) Framboidal iron oxide: chondrite-like material from the black mat, Murray Springs, Arizona. *Earth and Planetary Science Letters*, 319-320, 251-258.

Fayek M, Hull S, Anovitz L, Haynes CV Jr, Bergen L. (2008) Evidence of impact material and the extinction of the mega-fauna 12,900 years ago. American Geophysical Union, Fall Meeting 2008, abstract #PP13C-1469.

Feathers JK. (2003) Use of luminescence dating in archaeology. *Measurement Science and Technology* 14:1493-1509.

Ferraro D and Bergin K. (2007) *Talega Site Report.* Viejo California Associates, Mission Viejo, CA.

Fiacco RJ J., Palais JM, Germani MS, Zielinski GA, and Mayewski PA. (1993) Characteristics and possible source of a 1479 A.D. volcanic ash layer in a Greenland ice core. *Quaternary Research* 39, 267–273.

Firestone RB, *et al.* (2007) Evidence for an extraterrestrial impact 12,900 years ago that contributed to the megafaunal extinctions and the Younger Dryas cooling. Proc Natl Acad Sci USA 104:16016–16021.

Firestone RB, *et al.* (2010) Analysis of the Younger Dryas Impact Layer. Journal of Siberian Federal University. Engineering & Technologies 1 (2010 3) 30-62.

Florenskiy KP. (1963) Preliminary Results From The 1961 Combined Tunguska Meteorite Expedition. Tenth Conference on Meteorites in May 1962, *Meteoritica*, Vol. XXIII.

Folco L, *et al.* (2008) Microtektites from Victoria Land Transantarctic Mountains. *Geology*, Vol. 36, No. 4, 291-294.

Forman S. (2002) OSL Dating and Topper. Paper presented at the Allendale-Topper Conference, Columbia, South Carolina.

French BM. (1998) Traces of Catastrophe. LPI Contribution No. 954, 102-103.

Fullerton DS, Bush CA, Pennell JN. (2003) Surficial deposits and materials in the eastern and central United States (east of 102 degrees west longitude) *U.S. Geological Survey Geologic Investigations Series, I-2789*, Edition: 1.0, U.S. Geological Survey, Denver, CO.

Gao L-X, Yao Y, and Wang L. (2004) Research on sintered fly ash aggregate of high strength and low absorption of water. Proceedings of International workshop on Sustainable development and Concrete Technology, 151-157.

Genge M and Grady M. (1998) Melted micrometeorites from Antarctic ice with evidence for the separation of immiscible Fe-Ni-S liquids during entry heating. *Meteoritics &Planetary Science* 33, 425-434.

Genge M and Grady M. (1999) The fusion crusts of stony meteorites: Implications for the atmospheric reprocessing of extraterrestrial materials. *Meteoritics & Planetary Science* 34, 341-356.

Genge MJ, Grady M, and Hutchison R. (1997) The textures and compositions of fine-grained Antarctic micrometeorites: Implications for comparisons with meteorites. *Geochimica et Cosmochimica Acta*, Vol. 61, No. 23, 5149-5162.

Giere R, Carleton LE, and Lumpkin GR. (2003) Micro- and nanochemistry of fly ash from a coal-fired power plant. *American Mineralogist*, Volume 88, pages 1853–1865.

Gikunoo E. (2004) *Effect of Fly Ash Particles on the Mechanical Properties and Microstructure of Aluminium Casting Alloy A535.* Thesis, Department of Mechanical Engineering, University of Saskatchewan, CAN.

Glass BP and Koeberl C. (2006) Australasian microtektites and associated impact ejecta in the South China Sea and the Middle

Pleistocene supereruption of Toba. *Meteoritics & Planetary Science* 41, Nr 2, 305–326.

Glass BP, Huber H, and Koeberl C. (2004) Geochemistry of Cenozoic microtektites and clinopyroxene-bearing spherules. *Geochimica et Cosmochimica Acta* 69, 3971-4006.

Glass BP. (1969) Silicate Spherules from the Tunguska Impact Area: Electron Microprobe Analysis, *Science* 164, 547-549.

Glass BP. (1990) Tektites and microtektites: key facts and inferences. In: Nicolaysen LO and Reimold WU (Editors), *Cryptoexplosions and Catastrophes in the Geological Record, with a Special Focus on the Vredefort Structure*. 171: 393-404.

Glass, BP and Koeberl C. (1999) Ocean Drilling Project Hole 689B spherules and upper Eocene microtektites and clinopyroxene-bearing spherule strewn fields. *Meteoritics & Planetary Science 34*, 197-208.

Gnos E, *et al.* (2004) Pinpointing the Source of a Lunar Meteorite: Implications for the Evolution of the Moon. *Science*, Vol. 30530, 657-659.

Grachev AF, Korchagin OA, Tselmovich VA, Kollmann HA. (2008) Cosmic dust and micrometeorites in the transitional clay layer at the Cretaceous-Paleogene boundary in the gams section (Eastern Alps): Morphology and chemical composition. Izvestiya, *Physics of the Solid Earth*, Vol. 44, No. 7, 555–569.

Hallett DJ, Mathewes RW, and Foit FF Jr. (2001) Mid-Holocene Glacier Peak and Mount St Helens We tephra layers detected in lake sediments from southern British Columbia using high resolution techniques. *Quaternary Research*, 55: 284-292.

Haynes CV Jr, *et al.* (2010a) The Murray Springs Clovis site, Pleistocene extinction, and the question of extraterrestrial impact. *Proc Natl. Acad. Sci. USA*, 107(9), 4010-4015.

Hillman G, Hedges R, Moore A, Colledge S, and Pettitt P. (2001) New evidence of Lateglacial cereal cultivation at Abu Hureyra on the Euphrates. *The Holocene* 11, 4, 383-393.

Horton, JW, and Dicken CL. (2001) Preliminary Geologic Map of the Appalachian Piedmont and Blue Ridge, South Carolina Segment: U.S. Geological Survey, Open-File Report 01-298, CD.

Jablonska M and Smola-Danielowska D. (2003) Aluminosilicate particles in fly ash and atmospheric dust. Mineralogical Society of Poland special papers 22, 82-89.

Jewell RB and Rathbone RF. (2009) Optical Properties of Coal Combustion Byproducts for Particle-Size Analysis by Laser Diffraction. *Coal Combustion and Gasification Products*, Vol. 1, 1-7.

Jones AP, *et al.* (2005) Are there signs of a large Paleocene impact, preserved around Disko Bay, West Greenland?: Nuussuaq spherule beds origin by impact instead of volcanic eruption?, in Kenkmann, T., Hörz, F., and Deutsch, A., eds., Large meteorite impacts III: *Geological Society of America Special Paper* 384.

Kelly DC and Elkins-Tanton LT. (2004) Bottle-green microtektites from the South Tasman Rise: Deep-sea evidence for an impact event near the Miocene/Pliocene boundary. *Meteoritics & Planetary Science* 39, Nr 12, 1921–1929.

Keyte LM, Lukey GC, and van Deventer JSJ. (2004) The Effect of Coal Ash Composition on Properties of Wastebased Geopolymers. International Symposium of Research Students on Material Science and Engineering, Chennai, India.

Kilian R, Hohner M, Biester H, Wallrabe-Adams HJ, and Stern CR. (2003) Holocene peat and lake sediment tephra record from the southernmost Chilean Andes (53-55°S). *Revista Geológica de Chile*, Vol. 30, No. 1, p. 23--37.

Kirova OA and Zaslavskaya NI. (1966) Data characterizing the dispersed matter as recovered from the area of fall of the Tunguska meteorite. *Meteoritika*, 27, 119-127.

Koeberl C (2007) The geochemistry and cosmochemistry of impacts. In: *Treatise of Geochemistry*, Vol. 1 (ed. A. Davis), Elsevier, p. 1.28.1 -1.28.52.

Koeberl C and Glass BP. (1988) Chemical composition of North American microtektites and tektite fragments from Barbados and DSDP Site 612 on the continental slope off New Jersey. *Earth and Planetary Science Letters,* 87, 286 292.

Koeberl C and Sigurdsson H. (1992) Geochemistry of impact glasses from the K/T boundary in Haiti: Relation to smectites, and a new type of glass. *Geochimica et Cosmochimica Acta* 56, 2113- 2129.

Koeberl C, Brandstätter F, Niedermayr G, and Kurat G. (1988) Moldavites from Austria. Meteoritics 23, 325-332.

Koeberl C, *et al.* (2006) Uppermost Impact Fallout Layer in a Drillcore at the Bosumtwi Impact Crater (Ghana): A Preliminary Study. 37th Annual Lunar and Planetary Science Conference, March 13-17, 2006, League City, Texas, abstract no.1552.

Koeberl C, Kruger FJ, and Poag CW. (2001) Geochemistry of surficial sediments near the Chesapeake Bay impact structure and the search for source rocks of the North American Tektites. *Lunar and Planetary Science* XXXII.

Koeberl C. (1992) Geochemistry and origin of Muong Nong-type tektites. *Geochimica et Cosmochimica Acta* 56, 1033-1064.

Koeberl C. (1998) Identification of meteoritical components in impactites. In: *Meteorites: Flux with Time and Impact Effects;* Grady, M.M., Hutchison, R., McCall, G.J.H., and Rothery, D.A., (Eds.), Geological Society of London, Special Publication 140, 133-152.

Koeberl C. (2007) The geochemistry and cosmochemistry of impacts. In: *Treatise of Geochemistry*, Vol. 1 (ed. A. Davis), Elsevier, p. 1.28.1 -1.28.52, doi:10.1016/B978-008043751-4/00228-5.

Koeberl C., 1990. The geochemistry of tektites, an overview. In: L.O. Nicolaysen and W.V. Reimold (Editors), Cryptoexplosions and Catastrophes in the Geological Record, with a Special Focus on the Vredefort Structure. *Tectonophysics*, 171: 405-422.

Kolesnikov EM, Kolesnikova NV. (2010) Traces of cometary material in the area of the Tunguska impact (1908). *Solar System Research* 44, 110-121.

Kulik LA. (1940) The meteorite expedition to Podkamennaya Tunguska in 1939. *Comptes Rendus De L Academie Des Sciences De L Urss* 28, 596-600.

Kurat G, Koeberl C, Presper T, Brandstätter F, Maurette M. (1994) Petrology and geochemistry of Antarctic micrometeorites. *Geochimica et Cosmochimica Acta,* vol. 58, Issue 18, 3879-3904.

LeCompte MA, Goodyear AC, Demitroff M, Batchelor D, Mooney C. (2010) An Independent Review of the Younger Dryas Extraterrestrial Impact Hypothesis and its Recent Re-Evaluation by Surovell *et al.* 21st Biennial Meeting of the American Quaternary Association (AMQUA). Laramie, Wyoming.

Lee MY, Chen C-H, Wei K-Y, Iizuka Y, Carey S. (2004) First Toba supereruption revival. *Geology* 32, 61–64.

Lodders K and Fegley B. (1998) *The Planetary Scientist's Companion*. Oxford Univ. Press, Oxford, 314-316.

Luetke S, Deutsch A, Berndt J, Langenhorst F. (2008) Trace Elements in Ivory Coast Tektites, Microtektites, and Fallback Particles of the Lake Bosumtwi Impact Crater, Ghana: A LA-ICP-MS Study. 39th Lunar and Planetary Science Conference, (Lunar and Planetary Science XXXIX), held March 10-14, 2008 in League City, Texas. LPI Contribution No. 1391., p.1613.

Mahaney WC, *et al.* (2010b) Evidence from the northwestern Venezuelan Andes for extraterrestrial impact: The black mat enigma. *Geomorphology*, v. 116, iss. 1-2, p. 48-57.

Mahaney WC, *et al.* (2011a) Fired glaciofluvial sediment in the northwestern Andes: Biotic aspects of the Black Mat. *Sedimentary Geology*. 237, (1-2), 73-83.

Mahaney WC, *et al.* (2011b) Notes on the black mat sediment, Mucunuque Catchment, northern Mérida Andes, Venezuela. *Journal of Advanced Microscopic Research*, vol. 6, no. 3.

Mahaney WC, Krinsley D, Kalm V (2010a) Evidence for a cosmogenic origin of fired glaciofluvial beds in the northwestern Andes: Correlation with experimentally heated quartz and feldspar. *Sedimentary Geology*, v. 231, iss. 1-2, p. 31-40.

Mandal A and Sengupta D. (2006). An assessment of soil contamination around coal- based thermal power plant in India, *Environmental Geology*, 51 (3) 409-420.

Marini F and Raukas A. (2009) Lechatelierite-bearing microspherules from semicoke hill (Kiviõli, Estonia): contribution to the contamination problem of natural microtektites. *Oil Shale* 26(3), 415-423.

Mascarenhas-Pereira, MBL, Nath BN, Borole DV, Gupta SM. (2006) Nature, source and composition of volcanic ash in sediments from a fracture zone trace of Rodriguez Triple Junction in the Central Indian Basin. *Marine Geology,* vol.229, 79–90.

Maurette M, Hammer C, Reeh N, Brownlee DE, Thomsen HH. (1986) Placers of cosmic dust in the blue ice lakes of Greenland. *Science* (ISSN 0036-8075), vol. 233, Aug. 22, 1986, p. 869-872.

McDonough WF. (1998). Earth's core. *In: Encyclopedia of geochemistry.* Marshall, C.P. and Fairbridge, R.W. (Editors), Kluwer Academic Publishers, Dordrecht. 151-156.

McHugh CMG, *et al.* (1996) Upper Eocene tektites of the New Jersey continental margin, Site 904. In: Mountain G. S., Miller K. G., Blum P., Poag C. W. and Twichell D. C. (eds). Proceedings of the Ocean Drilling Program, Scientific Results. United States Government Printing Office, Washington, D.C. USA. 150: 241-265.

McHugh CMG., Snyder SW, Miller KG. (1998) Upper Eocene ejecta of the New Jersey continental margin reveal dynamics of Chesapeake Bay impact. *Earth and Planetary Science Letters.* 160 (3-4): 353-367.

McKeen RG, Lenke LR, Pallachulla KK. (1998), Mitigation of Alkali Silica Reactivity in New Mexico. Materials Research Center, University of New Mexico, Albuquerque, NM.

Melson WG, O'Hearn T, and Jarosewich E. (2002) A data brief on the Smithsonian Abyssal Volcanic Glass Data File. *Geochemistry Geophysics Geosystems*, Vol. 3 No. 4, 10.

Melson WG, O'Hearn T, Fredriksson K. (1988) Composition and Origin of Basaltic Glass Spherules in Pelagic Clay from the Eastern Pacific. *Marine Geology*, 83 (1988) 253-271.

Misra S, *et al.* (2009) Geochemical identification of impactor for Lonar crater, India. *Meteoritics & Planetary Science*, vol. 44, Issue 7, p.1001-1018.

Mittlefehldt DW. (2004). Achondrites. In: *Treatise on Geochemistry*. Holland, H.D. and Turekian, K.K. (Editors), Elsevier, Amsterdam. 291-324.

Moore AMT and Hillman GC. 1992. The Pleistocene to Holocene transition and human economy in Southwest Asia: the impact of the Younger Dryas. *American Antiquity* 57, 3, 482-494.

Moore AMT, *et al.* (1986) Radiocarbon accelerator (AMS) dates for the epipaleolithic settlement at Abu Hureyra, Syria. *Radiocarbon* 28(3): 1068-1076.

Moore AMT, Hillman GC, and Legge AJ. (2000) *Village on the Euphrates*. Oxford University Press: New York, 585 pages.

Muriithi GN, Gitari MW, Petrik LF. (2009) Brine Remediation using Fly Ash and Accelerated Carbonation. In: Water Institute of Southern Africa & International Mine Water Association: Proceedings, International Mine Water Conference, 671-679.

Murray AS and Wintle AG. (2000) Luminescence dating of quartz using an improved single-aliquot regenerative-dose protocol. *Radiation Measurements* 32 (1): 57-73.

Nataraja MC, Jayaram MA, Raikumar, CN. (2007) Inductive Classifying Artificial Network for Fly Ash Type Categorization. *Engineering Letters,* 14:1, EL_14_1_28.

Newsom HE. (1995) Composition of the Solar System, Planets, Meteorites, and Major Terrestrial Reservoirs. In *Global earth physics, a handbook of physical constants.* Edited by Thomas J. Ahrens. American Geophysical Union, AGU reference shelf Series, vol no 1, 159-189.

Nugteren HW, Butselaar-Orthlieb VCL, Izquierdo M. (2009) High Strength Geopolymers Produced from Coal Combustion Fly Ash. *Global NEST Journal*, Vol 11, No 2, 155-161.

Oymael S. (2007) Suitability of Oil Shale Ash as a Constituent of Cement. Oil Shale, Vol. 24, No. 1, 45–58.

Poag CW, Koeberl C, and Reimold WU. (2004) *The Chesapeake Bay Crater: Geology and Geophysics of a Late Eocene Submarine Impact Structure.* New York: Springer, 522 pages.

Povenmire H, Chance S. (1997) Tektite from Jenkins County, Georgia. 28th Annual Lunar and Planetary Science Conference, March 17-21, 1997, Houston, TX, p. 1135.

Povenmire H, Glass BP, Strange RL. (1994) Discovery and description of a Muong Nong-type Georgia tektite. Abstracts of the Lunar and Planetary Science Conference. 25th: 1101-1102.

Pigati, JS, *et al*. (2012) Accumulation of "impact markers" in desert wetlands and implications for the Younger Dryas impact hypothesis. *Proc. Natl. Acad. Sci. USA* (in press).

Prasad MS and Khedekar VD. (2003) Impact microcrater morphology on Australasian microtektites. *Meteoritics & Planetary Science* v.38, 1351-1371.

Prasad MS, Roy SK, Gupta A. (2010) Changes in abundance and nature of microimpact craters with distance from the proposed source crater location. Meteorit Planet Sci, 45, 6, 990-1006.

Provis JL, Duxson P, Harrex RM, Yong C-Z, Van-Deventer SJ. (2009) Valorisation of fly ashes by geopolymerisation. *Global NEST Journal* 11 (2) : 147-154.

Rawlings, RD, Wu, JP, Boccaccini, AR.(2006) Glass-ceramics: Their production from wastes-a review. J Materials *Science* 41 (3) 733 - 761.

Renssen H, Isarin RFB, Vandenberghe J. (2001) Rapid climatic warming at the end of the last glacial: new perspectives. *Global and Planetary Change* 30, 1-2, 155-165.

Robinson SA, Black S, Sellwood BW, Valdes PJ. (2006) A review of palaeoclimates and palaeoenvironments in the Levant and Eastern Mediterranean from 25,000 to 5000 years BP: setting the environmental background for the evolution of human civilisation. *Quaternary Science Reviews* 25, 13-14, 1517-1541.

Rochette P. (2008) Micrometeorites from the Transantarctic Mountains. *Proc Natl. Acad. Sci. USA* November 25, 2008 vol. 105 no. 47 18206-18211.

Schultz P. (2004) The Quaternary impact record from the Pampas, Argentina. *Earth and Planetary Science Letters* 219 (2004) 221-238.

Schultz PH, *et al.* (2006) The record of Miocene impacts in the Argentine Pampas. *Meteoritics & Planetary Science* 41: 749-771.

Scruggs, MA, Raab LM, Murowchick JS, Stone MW, Niemi TM. (2010) Investigation of Sediment Containing Evidence of the Younger Dryas Boundary (YPB) Impact Event, El Carrizal, Baja California Sur, Mexico. *Geological Society of America Abstracts with Programs*, Vol. 42, No. 2, p. 101.

Sheffer AA, Dyar MD, Sklute EC (2006) Lightning strike glasses as an analog for impact glasses: 57Fe Mössbauer Spectroscopy of Fulgurites. 37th Annual Lunar and Planetary Science Conference, March 13-17, 2006, League City, Texas, abstract no.2009.

Shoumkova AS. (2006) Physico-Chemical Characterization and Magnetic Separation of Coal Fly Ashes from "Varna," "Bobov Dol" And "Maritza-Istok I" Power Plants, Bulgaria: Physico-Chemical Characteristics. *Journal of the University of Chemical Technology and Metallurgy,* 41, 2, 175-180.

Simons DL, Shott MJ, Wright HT. (1984) The Gainey site: variability in a Great Lakes Paleo-Indian assemblage. *Archaeology of Eastern North America* 12, 266-279.

Sivakumar G, Mohanraj K, and Barathan S. (2009) Dielectric Study on Fly Ash Blended Cement. *E-Journal of Chemistry,* 6(1), 231-236.

Snelson DG, Kinuthia JM, Davies P, Chang S-R. (2007) Sustainable road construction in the United Kingdom: Combined use of waste tyres and PFA. The 9th International Conference, Modern Building Materials, Structures and Techniques, 168-173.

Son TH, Koeberl C. (2005) Chemical variation within fragments of Australasian tektites. Meteoritics & Planetary *Science* 40, Nr 6, 805–815.

Sponholz B, Baumhauer R, and Felix-Henningsen P. (1993) Fulgurites in the southern Central Sahara, Republic of Niger, and their palaeoenvironmental significance. The Holocene, 3,2, 97-104.

Sponholz B. (2004) Fulgurites as palaeoclimatic indicators—the proof of fulgurite fragments in sand samples. In Paleoecology of Quaternary Drylands, Lecture Notes in Earth Sciences, Felix-Henningsen P (ed), Springer, Berlin/Heidelberg, 102, pp. 73–78.

Sulc R. (2009) Effect of Water Ratio in Fly-Ash Concrete on the Process of Alkali Activation. In Mlady vedec [CD-ROM]. Košice: Technická universita v Košiciach, Stavebná fakulta.

Svetsov VV. (2006) Thermal radiation on the ground from large aerial bursts caused by Tunguska-like impacts. LPSC 37th, 1553.

Taylor LA, *et al.* (2002) Martian meteorite Dhofar 019: A new shergottite. *Meteoritics & Planetary Science* 37, 1107–1128.

Taylor S. (2002) Micrometeorites from the South Pole water well. Boulder, CO, USA: National Snow and Ice Data Center.

Taylor SR and McLennan SM. (1985) *The continental crust: Its composition and evolution.* Oxford: Blackwell Scientific Publications, 312 pages.

Towler MR, *et al.* (2002) Modelling of the glass phase in fly ashes using network connectivity theory. International Workshop on Novel Products from Combustion Residues, 240-245.

Trnka M and Houzar S. (2002) Moldavites: a review. *Bulletin of the Czech Geological Survey,* Vol. 77, No. 4, 283–302.

Uścinowicz G. (2009) Micro-scale magnetic grains from shallow water sediments of the Gulf of Gdańsk. *Journal of Oceanography and Hydrobiology*. Vol. XXXVIII, No.4, 21-30.

USGS. (2001) Geochemistry of soils in the US from the PLUTO database: U.S. Geological Survey, Reston, VA.

Vallier T, Bohrer D, Moreland G, McKee EE. (1977) Origin of basalt microlapilli in lower Miocene pelagic sediment, northeastern Pacific Ocean. *Geol. Soc. Am. Bull.,* 88: 787-796.

van Geel B, Coope GR, and van der Hammen T. (1989) Palaeoecology and stratigraphy of the Lateglacial type section at Usselo (the Netherlands). *Rev. Palaeobot. Palynol.* 60: 25-129.

Vasilyev NV. (1998) The Tunguska Meteorite problem today. Planetary and Space Sciences, v.46, no.2/3, p.129-150.

Walter M. (2011) An Exogenic Fulgurite Occurrence in Oswego, Oswego County, New York. Rocks and Minerals, Vol. 86, 3, 264-270.

Wang JW and Cheng TW. (2003) Production geopolymer materials by coal fly ash. Proceedings of the 7th International Symposium on East Asian Resources Recycling Technology, Tainan, Taiwan.

Ward CR, French DH, Jankowski J, Riley KW, Li Z. (2006) Use of coal ash in mine backfill and related applications. Research report, Cooperative Research Centre for Coal in Sustainable Development, Australia, 62.

Wasilewski P, and Kletetschka G. (1999) Lodestone - Natures Only Permanent Magnet, what it is and how it gets charged, Geophysical Research Letters 26(15), 2275-227.

Wasson J. (2003) Large aerial bursts; an important class of terrestrial accretionary events. *Astrobiology*, 3(1): 163-179.

Wasson JT and Moore K. (1998) Possible formation of Libyan Desert Glass by a Tunguska-like aerial burst. *Metoritics and Planet. Sci* 33, A163.

Wastegård S, Bjorck S, Grauert M, Hannon GE. (2001) The Mjauvøtn tephra and other Holocene tephra horizons from the Faroe Islands: a link between the Icelandic source region, the Nordic Seas, and the European continent. *The Holocene* 11,1 (2001) 101–109.

Weiss H, *et al.* (1993) The Genesis and Collapse of Third Millennium North Mesopotamian Civilization. *Science*, Vol. 261, 995-1003.

White DJ, Harrington D, Thomas Z. (2005) Fly ash soil stabilization for non-uniform subgrade soils, Volume I: Engineering properties and construction guidelines. Iowa State University, Ames, IA: Center for Transportation Research and Education Iowa State University.

Winkler HGF. (1979) *Petrogenesis of Metamorphic Rocks.* Springer-Verlag, New York, 334 pages.

Wittke JH, *et al.* (2012) High-temperature, Iron-rich Microspherules from Three Continents: Evidence for an ET Impact at the Younger Dryas Onset (12.9 ka). *Proc Natl. Acad. Sci. USA* (in review).

Wörner G and Schmincke H-U. (1984) Mineralogical and chemical zonation of the Laacher See tephra sequence (East Eifel, FRG). *Journal of Petrology,* Vol. 25, Part 4, 805-835.

Wu Y. (2011) *Origin and Provenance of Magnetic Spherules at the Younger Dryas Boundary*. Thesis, Dartmouth College, NH.

Yamada K, *et al.* (2001) Removal of Phosphate from Aqueous Solution by Crystallization Using Coal Fly Ash. 2001 International Ash Utilization Symposium, Center for Applied Energy Research, University of Kentucky, Paper #7.

Yijin L, Shiqiong Z, Jian Y, Yingli G. (2004) The Effect of Fly Ash on the Fluidity of Cement Paste, Mortar, and Concrete. Proceedings of the International Workshop on Sustainable Development and Concrete Technology Beijing, China.

Zbik M. (1984) Morphology of the Outermost Shells of the Tunguska Black Magnetic Spherules. *J. Geophys. Res.,* vol. 89, B605-B611.

Zolensky, ME, Koeberl, C. (1991) Why are blue zhamanshinites blue? Liquid immiscibility in an impact melt. *Geochimica et Cosmochimica Acta* (ISSN 0016-7037), vol. 55, May 1991, p. 1483-1486.